

A Planar Hopping Robot with One Actuator:

Design, Simulation, and Experimental Results

Akihiro Sato

Department of Mechanical Engineering,
McGill University, Montreal, Canada

June 2004

A thesis submitted to the Faculty of Graduate Studies and Research in partial fulfillment of the requirements of the degree of Master of Engineering

©Akihiro Sato, 2004

Abstract

Animal legs are much more complex than necessary for running on horizontal surfaces. Past research shows that, despite their complexity, they act essentially like simple pogo sticks or “Spring Loaded Inverted Pendulums” (SLIP). Only recently was it discovered that SLIP possesses some degree of passive stability. In this research, the possibility of the realization of the SLIP model is investigated first in numerical simulation. Next, a small one-legged hopping robot with only one actuator is designed and built, and a simple hopping controller is implemented, which results in running with approximately 0.80 *m/s* (6.7 leg lengths per second). Comparison between simulation and experimental data is undertaken, and the stability of the resulting motion is investigated.

Résumé

Les pattes animales sont beaucoup plus complexes que ce qui est nécessaire pour courir sur des surfaces horizontales. En effet, des recherches passées montrent que malgré leur complexité, elles agissent essentiellement comme de simples « pogo sticks » ou « Spring Loaded Inverted Pendulums » (SLIP). Il a été découvert récemment que le SLIP possède un certain degré de stabilité passive. La présente recherche étudie tout d'abord la possibilité de réalisation du SLIP à l'aide de simulations numériques. Ensuite, un petit robot à une patte et un actuateur est développé et conçu, et un contrôleur de bonds est implémenté. Avec ce contrôleur, le robot peut atteindre une vitesse de 0.80 m/s , ce qui correspond à 6.7 longueurs de patte par seconde. Finalement, les résultats simulés et expérimentaux sont comparés et la stabilité du mouvement du robot est étudiée.

Acknowledgments

I'm happy that I have studied in the Ambulatory Robotics Laboratory and studied at McGill University and lived in Montreal. First of all, I thank the people who gave me the chance:

- My family: I thank for their understanding and support.
- Prof. Ken Tomiyama, ex-supervisor: He encouraged my plan to study abroad. His engineering courses using English were not only good lectures themselves but also good preparation for courses in English at McGill. His recommendation letter for my application was strong.
- Prof. Martin Buehler, supervisor: He decided to take me only after I went to his office twice. He gave me a big chance. I thank him for his generous personality. I hope I worked hard enough and returned the favor.

I thank the following people for leading and helping my research:

- Prof. Martin Buehler: I have been impressed not only by his research capabilities but also by his passion to continue doing research. This stimulates my work. His knowledge and experience in legged robots also gave me a lot. I am really lucky that I have had his supervision and I might be his first and last Japanese student.
- Ioannis Poulakakis: He is another “supervisor” of mine. He mainly helped with the theoretical aspects of dynamics analysis and control in my research. I thank him for his guidance throughout my studies. He is the guy who can study if there is no exam.
- Neil Neville: He proof-read Chapters 1 and 6. We sometimes had long discussions on my detail questions. His advice helped with the empirical tuning of PD gains and filters.
- James A. Smith: He proof-read Chapters 2 and 5 critically. Thanks for the cakes with the nicest care. He helped with the circuit for an IR sensor.
- Don Campbell: His sense of mechanical dynamics gave me hints for my robot simulation. Impressive that he is an electrical engineer. He designed a level

shifter between a D/A interface card and a motor amplifier on my first experimental setup.

- Dave McMordie: He provided the info and parts of the end-less potentiometers used on my experimental setup. He is one of the two “McGyver” persons I know.
- John Sheldon: He proof-read Chapters 1, 3, and 4 and the first version of the IROS 2004 paper. I was honored to talk about Japan.
- Evgeni Kiriy: He proof-read Chapter 1. He is the only perfectionist I ever met.
- Chris Prahacs: He proof-read Chapter 7. He amazingly keeps up with tight schedules.
- François Deschênes: He wrote the French abstract. He is my French teacher for bars. He was my partner on the red-flag team.
- Christine Georgiades: Her thrust measuring setup was a good reference for my setup. She is not afraid to study new fields.
- Francis: He got three Acco binders for me. Thanks for his two comments in and after my final presentation.
- Carl Steeves: My servo system is based on his lecture and notes on a motor drive system. I learned that one could become really good by asking good questions to other people.
- Rene Sutton Pronovost & Chris Owen: They built the main frame of the mechanical setup of the planarizer system. Discussions with them propelled my work progress as well.
- Shane Saunderson: He edited one of the two videos I used in my final presentation. He proof-read Chapter 5. I agree with his opinion about Vegetarian tofu, but I should have served real, raw tofu.
- Seigo Harashima: His help with the driver code for an AD/DA card was a key point to complete my experimental platform.
- Yunig Zhang: He helped my understanding of mechanical dynamics, especially in friction and system identification.
- Danny Chouinard & Jan Binder: Thanks for the great computer network administration. I sometimes came across their holiday work.
- Prof. Meyer: Nahon: His care saved a lot of my time to do paperwork for thesis submission.

- Vanessa Cadrin: She proof-read Chapter 2 and helped editing the style of this thesis.

Table of Contents

Abstract	ii
Résumé	iii
Acknowledgments	iv
Table of Contents	vii
List of Figures	x
List of Tables	xi
CHAPTER 1: INTRODUCTION.....	1
1-1. Motivation	1
1-2. Goal.....	2
1-3. Related work	3
1-3-1. SLIP model.....	3
1-3-2. Past work in ARL.....	4
CHAPTER 2: DESIGN.....	6
2-1. Platform requirements.....	6
2-2. Mechanical parameter designs.....	7
2-2-1. Body mass.....	7
2-2-2. Leg spring stiffness.....	8
2-2-3. Leg length.....	13
2-3. Controller design.....	15
2-3-1. State machine	15
2-3-1-1. Phases and events	16
2-3-1-2. States	17
2-3-1-3. State machine.....	18
2-3-1-4. Phase detection.....	19
2-3-2. Leg control.....	20
2-3-2-1. Leg angles at touchdown and lift-off.....	20
2-3-2-1-1. Forward speed and sweeping range	20
2-3-2-1-2. Sweeping mid-angle.....	23
2-3-2-1-3. Tuning of touchdown, lift-off, and sweeping mid-angles	24
2-3-2-1-4. Energy distribution	25
2-3-2-2. Forward speed	27
2-3-2-3. Apex height.....	29
2-3-2-4. Stabilization.....	30
2-3-2-5. Control scheme	31
2-3-2-5-1. Overview.....	31
2-3-2-5-2. Reflex control and step input.....	33

2-3-2-5-3. Angle control	34
2-3-2-5-4. Stance torque	34
2-3-2-5-5. Spring-like response	34
2-3-2-5-6. Adjustable response shape	35
2-3-2-5-7. Comparison to Raibert's three-part controller.....	35
CHAPTER 3: SIMULATION IMPLEMENTATION	37
3-1. Dynamics Models	37
3-2. Methods	40
3-2-1. Numerical simulation settings.....	40
3-2-2. Stability analysis	40
3-2-2-1. Analysis tool selection.....	40
3-2-2-2. Stability definition	41
3-2-2-3. Lenient criteria for convergence.....	42
3-2-2-4. Robustness	42
3-2-2-5. Phase plots and limit cycles.....	43
3-2-2-6. Transition plots and regions of attraction	43
CHAPTER 4: SIMULATION RESULTS	45
4-1. Motion in the Sagittal Plane.....	45
4-2. Phase Plot.....	46
4-3. Transition plot and Region of Attraction	48
4-4. Summaries	49
CHAPTER 5: EXPERIMENTAL SETUP	50
5-1. Mechanical Structure.....	50
5-1-1. Overview.....	50
5-1-2. Planarizer	53
5-2. Computer & Electronic System	54
5-2-1. Structure	54
5-2-2. Hardware components.....	55
5-2-2-1. Computers.....	55
5-2-2-2. Operating Systems	56
5-2-2-3. Interface card.....	56
5-2-2-4. Actuator	57
5-2-2-5. Motor amplifier.....	58
5-2-2-6. Distance sensor.....	59
5-2-2-7. Rotational position sensors.....	60
5-2-3. Controller code	62
5-2-3-1. Overview	62
5-2-3-2. Lowpass filters.....	63
5-2-3-3. PD gains.....	63
5-2-3-4. Commanded current limitation	63
5-3. Methods	64

CHAPTER 6: EXPERIMENTAL RESULTS.....	65
6-1. Motion in the Sagittal Plane.....	65
6-1-1. High frame-rate video.....	66
6-1-2. Body height vs. horizontal position	69
6-1-3. Body height vs. time	70
6-1-4. Horizontal position vs. time	72
6-1-5. Forward speed vs. time.....	72
6-1-6. Leg length vs. time	74
6-1-7. Summary in hopping motion.....	77
6-2. Servo performance	77
6-2-1. Commanded and actual leg angles	77
6-2-2. Desired, commanded, and actual current	79
6-2-3. Torque-speed curve	80
6-2-4. Summary of motor control performance.....	82
6-3. Stability	84
6-3-1. Phase plot of vertical height.....	84
6-3-1-1. Stance phase and energy balance	85
6-3-1-2. Flight phase and leg model error	85
6-3-1-3. Symmetry.....	86
6-3-2. Phase plot of leg angle	86
6-3-2-1. Commanded and actual angles and limit cycle	87
6-3-2-2. Symmetry.....	88
6-3-3. Phase plot of leg length	88
6-3-3-1. Error.....	89
6-3-3-2. Symmetry.....	90
6-3-4. Vertical position phase portrait time evolution.....	91
6-3-5. Transition plot.....	92
6-3-6. Experimental region of attraction	93
6-3-7. Summaries in stability	95
CHAPTER 7: CONCLUSIONS	96
7-1. Conclusions	96
7-2. Future work.....	97
BIBLIOGRAPHY	99

List of Figures

Figure 1.	Spring Loaded Inverted Pendulum (SLIP) model. (Reproduced from [15]).....	2
Figure 2.	Natural frequency during a complete stride vs. body mass of SLIP and vs. leg length.....	10
Figure 3.	Cycle of the two phases with the two phase transition events	17
Figure 4.	State machine for a planar one-legged hopping robot. The five states are shown along with the events that trigger the state transitions. Reproduced from [32]	18
Figure 5.	SLIP model in stance phase [16].....	21
Figure 6.	Toucdown leg angle vs. desired forward speed for $m=0.54\text{ kg}$, $k=193\text{ N/m}$, $r_0=0.120\text{ m}$	22
Figure 7.	Two cases of the hip torque contribution: (a). the most input force directs forwards due to a wide leg angle at lift-off, (b). the most input force directs upwards due to a narrow leg angle at lift-off Reproduced from [15]	24
Figure 8.	Flowchart of the author’s entire control scheme.....	32
Figure 9.	Hopping motion in the Sagittal Plane	45
Figure 10.	Phase plot for the vertical position of the COM.....	47
Figure 11.	Vertical position and speed trajectory	47
Figure 12.	Convergence transition	48
Figure 13.	Region of attraction in simulation	49
Figure 14.	Entire view of the CAD design of the robot with a planarizer	51
Figure 15.	Entire view of the actual robot and planarizer with a planarizer	52
Figure 16.	Close view of the robot.....	52
Figure 17.	Raibert’s circular-boom-type planarizer with 3 DOF for Planar Biped [16]	54
Figure 18.	Computer & Electronic System structure.....	55
Figure 19.	PCI-3523A from Interface Corporation	57
Figure 20.	HS-5735MC from Hitec RCD USA, Inc.....	58
Figure 21.	Servo amplifier 25A8 from Advanced Motion Controls.....	59
Figure 22.	RL50 infrared sensor from STM	59
Figure 23.	Endless potentiometer N-15 from Piher	61
Figure 24.	Conductive Plastic potentiometer CP-2FK from Midori America Corporation	61
Figure 25.	Diagram of the controller in the entire system loop.	62
Figure 26.	Slow-motion snapshots of hopping motion from an apex to the next apex	68
Figure 27.	Vertical position vs. horizontal position for the COM with a large error IC.....	69
Figure 28.	Vertical position of the COM over time	71
Figure 29.	Horizontal position over time	72
Figure 30.	Forward speed over time	73
Figure 31.	Leg length with error over time	74
Figure 32.	Leg length over time.....	76
Figure 33.	Commanded and actual leg angles vs. time.....	78

Figure 34.	Desired, commanded, and actual current vs. time: positive current protracts the leg in flight and negative one retracts it in stance	80
Figure 35.	Torque-speed curve of the motor.....	81
Figure 36.	Phase plot for the vertical position of the COM.....	84
Figure 37.	Phase plot for leg angle	87
Figure 38.	Phase plot for leg length	89
Figure 39.	Vertical position phase portrait time evolution	91
Figure 40.	Transition plot for an IC with large error	93
Figure 41.	Converged transitions for 10 IC's	94

List of Tables

TABLE I.	Part masses for future implementation.....	8
TABLE II.	Animal data reproduced from [14] with dimension-less speeds	10
TABLE III.	Approximate leg lengths, speeds, and dimension-less speeds of legged robots. 29	
TABLE IV.	Parameters for dynamics models	39
TABLE V.	PD gains	63

Chapter 1: Introduction

1-1. Motivation

Practical mobility of machines using legs has been desired for environmental surveillance and rescue activities [1], [2]. The main reason is that wheeled vehicles often cannot negotiate rough terrain when they are sent to such environments as mountain ranges and collapsed urban city structures [3], [4]. Hence, robotic legged locomotion has been studied for many years [5], [6], [7], [4], but still this field is developing. The work detailed in this thesis deals specifically with robotic running.

If we first look to nature, animals run on rough terrain with high negotiating performance. For instance, cheetahs can gallop at 31 m/s and red kangaroos can leap at 16 m/s (converted from [8]). Hence, it is a good idea to draw insight from animal locomotion. Animals are redundant in kinematics, actuation, and control [9]. For three decades, researchers in fields related to biomechanics have been trying to understand the running motion of animals by simplifying models of animals and researchers in robotics have been exploiting it for designing and controlling robots. For three decades, animal running models have been described using the Spring Loaded Inverted Pendulum (SLIP) [10], [11], [12], [13], [14], [9]. The SLIP model consists of a point-mass on a linearly springy leg and represents the dynamics of the center of mass (COM) of a running

animal and the *virtual* springy leg from the COM to the foot point on the ground, as in Figure 1. The COM of an animal is considered, so even the masses of legs are counted in the COM of the whole body. As a result, the leg of the SLIP model is not a physical leg but a conceptual leg with the distance between the COM location of the body and the location of the foot. Since it is conceptual or “virtual,” it is often treated as a mass-less leg in modeling and control. The virtual leg behaves as if it was a linear spring. (Note that it does not mean that each muscle in animal legs behaves in the same way as a linear spring.) The SLIP model motivated the design of the robot used in this research.

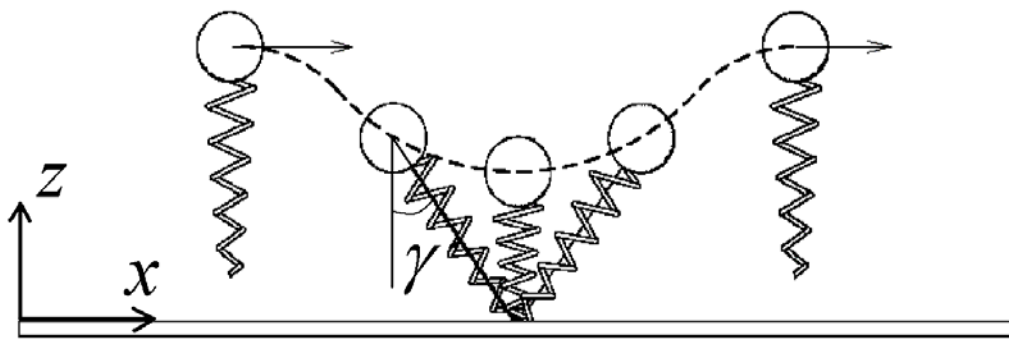


Figure 1. Spring Loaded Inverted Pendulum (SLIP) model. (Reproduced from [15])

1-2. Goal

The SLIP model was adopted as a basis of the robot design and set the goals of this research as follows:

- Feasibility study of the realization of the SLIP model
- Design and construction of a SLIP robot hopper with one actuator
- Experimental implementation of a simple controller on the SLIP.

As a result, we achieved the following:

- Experimental validation of the SLIP model

- Demonstration of a robust hopping robot with only one actuator at the hip of the leg.

1-3. Related work

1-3-1. SLIP model

The SLIP model has been used for 20 years among robotics researchers [16], [17], [18], [19], [74]. Raibert and his co-workers at Carnegie Mellon University (CMU) and Massachusetts Institute of Technology (MIT) established the first milestone by using the SLIP as a dynamics model of his hopping robots [16], and since then, most hopping and running robots use Raibert's controller based on SLIP models. One good example is a simulation of the bipedal running control of a full-sized and human-shaped robot, HRP1, using a SLIP model [20]. Though the robot has two arms and two legs with many degrees of freedom (DOF), they are controlled in such a way that the COM and its virtual leg from the COM to the foot contact point with the ground can be treated as those in a SLIP model. As a result, the robot with complex mechanisms and dynamics is controlled using a two-DOF model when it is on the ground and a one-DOF model when it is in the air. This leads to a successful running with a simple controller although it cannot be implemented due to motor torque limitations of existing technologies.

Though there has been extensive use of SLIP in the modeling and control of legged robots, the SLIP itself has never been developed and validated experimentally. In other words, many researchers have applied the SLIP model to their robots with complex mechanisms, but no robot whose kinematics is the same as the SLIP model has been constructed and experimented. To date, the Bow Leg hopper [17] at CMU is one of the closest in its design to the SLIP model. It has a passive compliant leg though it is a nonlinear curved fiberglass sheet spring, instead of a linear spring in the SLIP model. Moreover, its COM is located below the hip to allow the body to be self-righting while the SLIP model has its COM located in the hip joint. Therefore, this robot cannot be regarded as a realization of the SLIP model.

The SLIP is the minimum model for running [9], [10], [21]. It has two DOF of translation in the sagittal plane as in Figure 1. (The sagittal plane lies in the median plane dividing an animal into front and back halves and is perpendicular to the lateral plane and the horizontal plane.) Since the body is represented by a point mass at the COM, its inertia and pitch angle are not considered. The SLIP has only one actuated joint at the hip, which is coincident with its COM of the body. The compliant leg can be regarded as a prismatic joint with a spring while the leg is in contact with the ground, but it is unactuated. Construction will be inexpensive, control will be easier, and efficient locomotion might be achieved if a robot can run using only one actuator. The simple mechanism of a SLIP should be sufficient for the running motion alone [9].

The SLIP dynamics are naturally stable in the sense of its balance and do not require active balancing control provided that the leg can be brought at a desired angle at touchdown [22], [23], [24]. Due to this *self-stability* property, the control of the robot designed after the SLIP model can be simplified. Details are discussed later in section 2-3-2-4. *Stabilization*. Note that only recently was this property discovered in the SLIP, though McGeer simulated the same idea on a bipedal robot model two decades ago [25].

The author's robot is designed based on these features and the advantages studied in the past research work.

1-3-2. Past work in ARL

The author's robot is highly inspired by the robots built in the Ambulatory Robotics Laboratory (ARL) at McGill University. The SLIP model is successfully used in modeling and control of all the following robots:

- MONOPOD II: demonstrated that two electrical motors are sufficient for a running one-legged robot [26].
- Scout II: demonstrated that one electrical motor per leg allows for maneuverability in quadruped bounding [27]

- RHex: demonstrated that one electrical motor per leg and PD control for leg angle is sufficient for six-legged locomotion [28], [29].

These achievements in ARL have inspired the author and empowered him to achieve his research goals listed before.

Chapter 2: Design

Our robot is designed as a realization of the Spring Loaded Inverted Pendulum (SLIP) model. In order to do numerical simulation for investigating whether there is a possibility to realize a SLIP, the mechanical parameters of the SLIP are determined and a simple controller is prepared. After the simulation confirms the possibility, those parameters and controller are implemented on an actual experimental setup.

This Chapter begins with the platform requirements for realizing a SLIP-type, one-legged hopping robot. Then, the mechanical parameter designs are explained. Lastly, a simple controller for hopping is described.

2-1. Platform requirements

Here is the list of the requirements for the realization of a SLIP:

- One leg
- One hip joint, one prismatic joint

- Only one actuator in the hip
- One passive spring in the leg
- Nearly mass-less leg or a leg with negligible mass
- Center of mass (COM) of the body at the hip joint point
- No pitch angle motion of the body (i.e. the ideal SLIP has a point-mass body)
- 2D constraint (i.e. operation in the vertical plane).

2-2. Mechanical parameter designs

In this section, the author explains the decision procedure of mechanical parameters. The SLIP model consists of a point-mass with a springy leg. Therefore, there are three mechanical parameters to be determined in order to build a SLIP robot: mass, spring stiffness, and leg length.

2-2-1. Body mass

Since the robot is a prototype of a power-autonomous robot, the following things are considered.

A servo, a leg, and structural parts cannot be removed from robot components for an experimental setup. The sum of those masses is the minimum value possible for body mass. The total mass for those essential components is 0.320 *kg* (Refer to *Chapter 5: Experimental setup* for details.).

The prototype robot does not have to have an embedded computer, motor amplifiers, batteries, etc. onboard. Considering the case of a power-autonomous platform, however, the masses for those components have to be taken into account. TABLE I provides an idea of those masses:

TABLE I. PART MASSES FOR FUTURE IMPLEMENTATION

Part name	Manufacturer	Mass (kg)
PC104 embedded computer	VersaLogic	0.185
Flash car board	VersaLogic	0.175
I/O board	VersaLogic	0.090
Power supply board	VersaLogic	0.300
Motor amplifier	iXs Research Corp.	0.035
R/C car 6-cell battery pack	Panasonic	0.360

An aluminium block is attached for the future implementation of a motor amplifier and an embedded computer on the robot. It weighs 0.220 *kg*. The total mass of the body m is 0.540 *kg*.

2-2-2. Leg spring stiffness

The leg spring stiffness can be selected via the robot's desired stance duration. The stance duration can be approximated by half the resonant period of the spring vibration, which can be calculated from the natural frequency of the robot's vertical spring-mass dynamic model.

The maximum value of the spring constant is bounded by the angular speed of the actuator and the stance duration for posture control and energy compensation while the minimum value is bounded by the leg travel length. However, there is no generally used formula in robotics that uniquely derives a spring constant. When it comes to the selection of the spring constant value, it cannot be easily specified if only the maximum and minimum boundaries are known. Hence, the author uses findings in physiology as guidance in order to determine the value.

The model commonly used to explain the animal motion using the idea of a linear spring is called the Spring Loaded Inverted Pendulum (SLIP) model. The idea of a virtual spring in the animal leg came up among physiology and biomechanics papers [10], [11], [12], [13], [14], [9]. Researchers in the field took data from running animals

and concluded that the COM motion of running animals is explained using a linear spring for each one. In these experiments, the equivalent spring constants are obtained using the maximum ground force and the distance between the COM position and the support foot position when the virtual line is vertical. These sets of data and equations, especially the ones related to the natural frequency of running animals for this section, are considered.

The spring constant of the SLIP model is one of the two values that dominate the natural frequency of its mechanical vibration. Therefore, the spring constant very much affects the frequency of locomotion cycle. Hence, the author first seeks a value for the natural frequency of the platform, and then he uses it in order to obtain a spring stiffness value.

The author formulated two equations for obtaining the natural frequency during a complete stride of the equivalent size (mass and length) of animals, by plotting Farley's *et al* experimental data [14] in Figure 2. The data are in TABLE II (The table has an additional column for dimension-less speeds, so they can be compared to those of robots in TABLE III.). One is the relation to the body mass and the other is the relation to the leg length:

$$f_n = 3.0m^{-0.19} \quad (1)$$

$$f_n = 1.0r_0^{-0.58} \quad (2)$$

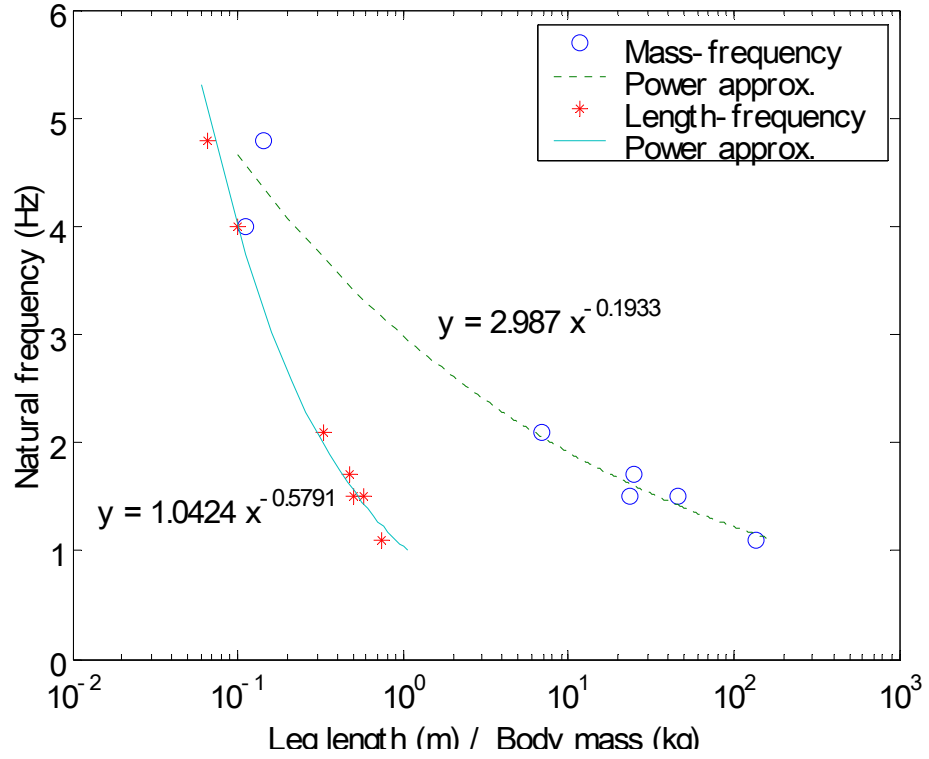


Figure 2. Natural frequency during a complete stride vs. body mass of SLIP and vs. leg length

TABLE II. ANIMAL DATA REPRODUCED FROM [14] WITH DIMENSION-LESS SPEEDS

Animal	Body mass M[kg]	Leg length L0[m]	Speed u[m/s]	Leg-length per sec (1/s)
Kangaroo rat	0.112	0.099	1.8	18.2
White rat	0.144	0.065	1.1	16.9
Tammar wallaby	6.86	0.33	3.0	9.1
Dog	23.6	0.50	2.8	5.6
Goat	25.1	0.48	2.8	5.8
Red kangaroo	46.1	0.58	3.8	6.6
Horse	135	0.75	2.9	3.9

From the first equation,

$$f_n = 3.4 \text{ Hz for } m = 0.5 \text{ kg} \quad (3)$$

and

$$f_n = 3.0 \text{ Hz for } m = 1.0 \text{ kg} . \quad (4)$$

Too high a frequency is not desirable since the leg is physically swung forwards and swept backwards in a hopping cycle and the actuator performance is bounded. Also, too high a frequency reduces the stance time, and as a result, the duration to inject energy into the spring potential energy and into the forward speed for kinetic energy is reduced. This sets an upper limitation on frequency and spring stiffness. Consequently, it would be reasonable to use 3 Hz as a start. The rule of thumb used in the ARL is 2 Hz for the natural frequency for a hopping locomotion [30]. It stems from many years of experience working with compliant legs. However, the mass values of all the past robots are much heavier. For instance, RHex approximately weighs 8.0 kg. If the author calculates its natural frequency based on Eq. (1) and 8.0 kg of mass, then the frequency referred to the equivalent size of animals is 2.0 Hz. This is exactly the same value as the rule of thumb in ARL. Therefore, it might be safe to say that the desired natural frequency is not a constant value such as 2.0 Hz but is a variable value obtained using Eq. (1). The proof of this suggestion is put to future work, and here the author concentrates on the experiment in one specific size. The natural frequency and the natural angular frequency can be expressed in a spring constant and a mass:

$$\begin{aligned} f_n &= \frac{1}{2\pi} \omega_n \\ &= \frac{1}{2\pi} \sqrt{\frac{k}{m}} \end{aligned} \quad (5)$$

or

$$k = (2\pi f_n)^2 m . \quad (6)$$

This formula provides 192 N/m and the closest value among off-shelf springs from Associated Spring Raymond is 193 N/m. Hence, the spring stiffness of the leg spring is 193 N/m.

Assuming that the effects of the gravitational force and the force that comes from hip torque are negligible, the estimated stance duration T_s is half the resonant period of the spring-mass vibration:

$$\begin{aligned}
 T_s &= \pi \sqrt{\frac{m}{k}} \\
 &= \pi \sqrt{\frac{0.54}{193}} \\
 &= 0.165 \text{ s}
 \end{aligned} \tag{7}$$

These calculations are valid only for vertical hopping but are used for to approximate planer hopping. The reliability of this approximation is demonstrated in [16]. Closed form solutions for the stance duration of non-vertical hopping are not known [31], [32].

A pre-deflection value is set so that the spring is slightly extended at the rest length of the leg. This eliminates most of spring chattering. It is good to reduce chattering phenomena after the lift-off impact. If it is severe, the spring continues to vibrate in the flight phase, i.e. there will be more than one time of the impact to the stopper.

To reduce the effect of lost energy during touchdown impact, the existence of a spring along the leg is very effective as well. In general, if the vertical speed at touchdown is high, the impact dynamics has to be considered in order to have a good understanding of a robot's dynamics [33], [34]. However, if a spring whose axis is along the leg is used and if its stiffness is small enough, it can be assumed that the impact loss is almost negligible [25]. Thus, a soft spring and a small pre-deflection are better on this purpose.

2-2-3. Leg length

The effective leg length of the robot at rest r_0 is 0.120 m. It is the maximum distance between the tip of the toe and the joint axis of the hip. In the flight phase, the leg length is kept at rest, and in the stance phase, the leg is shortened as the deflection of the spring increases.

The leg length design has the following requirements:

- The prismatic joint travel must be long enough that the body will not hit the bottom end of the travel during leg compression
- The leg length must be short enough that the motor torque can propel the robot with a torque lower than the stall torque
- The leg length must be long enough that the desired forward speed is achieved at a motor speed slower than the no load speed.

The author starts with the 1st requirement because the 2nd and 3rd requirements are the matters strongly coupled with the hopping controller. Thus, the latter two are more considered in simulation and experiment if the value from the 1st requirement is not successful.

The necessary travel is calculated using the energy conservation law for vertical hopping. Although planar hopping is the issue at hand, this approximation using vertical hopping is reasonable according to Raibert [16]. At the *apex* (highest position in flight), the vertical speed is zero and the spring deflection is also zero. At the *bottom* (lowest point in stance), the vertical speed is zero. Therefore, the following equation is formulated for a vertical hopping system from the conservation law:

$$mgz_{apex} = mgz_{bottom} + \frac{1}{2}k\delta_{bottom}^2 \quad (8)$$

where z_{apex} is the height at apex, z_{bottom} is the height at bottom, and δ_{bottom} is the spring deflection when the body is at bottom. Owing to the dimension of the servo casing, the height at bottom z_{bottom} has to be higher than 0.025 m . Otherwise, the servo casing will hit the ground during the stance phase. That is why the desired height at bottom is set to be 0.050 m with a small margin. The reason that a large margin is not desirable is that it would go against the 2nd requirement above. It would result in a long leg, which might create too large a counter-moment from ground reaction during stance. From Eq. (8),

$$\delta_{bottom} = \sqrt{\frac{2mg(z_{apex} - z_{bottom})}{k}} \quad (9)$$

The spring deflection δ_{bottom} becomes 0.081 m if the desired bottom height is 0.050 m the desired apex height is 0.170 m . Here, the author sets the target spring deflection at the bottom $\delta_{bottom,desired}$ to be 0.080 m . Now the rest length of the leg r_0 can be obtained since vertical hopping is argued:

$$r_0 = z_{bottom,desired} + \delta_{bottom,desired} = 0.120\text{ m} \quad (10)$$

The designed leg length at rest is 0.120 m .

The value obtained from the energy conservation law in the vertical hopping to some extent agrees with the ones from two of Farley's et al formulas [14]. In that paper, the formula for the relation between mass and leg length is

$$r_0 = 0.16m^{0.33} \quad (11)$$

For the mass of 0.54 kg , the leg length of the equivalent animal size would be 0.131 m .

The formula for the relation between the leg length and the natural frequency is Eq. (2). Transforming it for r_0 ,

$$r_0 = f_n^{-\frac{1}{0.58}} \quad (12)$$

For the natural frequency of 3.0 Hz, r_0 is 0.150 m. Because it is safer to use a short leg in order to avoid a large counter-moment from the ground reaction, these values are put aside for the time being.

In summary, the leg's rest length r_0 is set at 0.120 m so that the leg has the necessary prismatic joint travel for desired hopping height of 0.170 m. The sufficiency of the hip torque and speed of the leg is to be empirically confirmed.

2-3. Controller design

In this section, a locomotion controller is designed. It consists of a state machine for a locomotion cycle and methods for controlling the motion based on the states found in the state machine. A state machine is defined by the states that describe the conditions of the robot and the events that describe the transitions of the conditions. In the author's state machine, each state has one control method for leg actuation.

2-3-1. State machine

A *state machine* is a framework for describing discrete descriptions under which a system finds itself ("states") and specific actions which are taken based on these states. The transitions of states are based on "events." In this section the state and action elements of the state machine are described.

2-3-1-1. Phases and events

In general, legged robots are event-driven intermittent dynamical systems. They change their dynamical characteristics depending on their leg conditions, i.e. whether or not their legs are on the ground. For instance, legged robots are often modeled as a manipulator when only one leg is on the ground, a closed-chain mechanism when more than one leg are on the ground, and a floating mechanism when no leg is on the ground.

Those conditions are called *phases* in the field of legged locomotion [16]. *Stance phase* is a phase in which at least one leg is on the ground and the leg supports the body and propels the body to keep the locomotion. Some researchers call it *double-stance phase* if two legs of a multi-legged robot are simultaneously on the ground [15]. In the field of physiology, some researchers call it ground contact phase, instead. *Flight phase* is a phase that no leg is on the ground and the whole body is in the air. Some call it aerial phase, instead.

In the case of a one-legged hopping robot, there are only two conditions for state change: either the leg is on the ground or it is not. If the leg is on the ground, it is called stance phase. If the leg is off the ground, it is called flight phase. The phase transitions are driven by two *events*: touchdown and lift-off. Touchdown happens as an event from flight into stance. Lift-off occurs from stance into flight. The robot repeats the cycle of shifting phases and keeps it as long as it is stable. As a result, a one-legged hopping robot must be in either of these two phases, and its phase determines the dynamical characteristics of the robot.

Figure 3 shows the cycle of the two phases with the two phase transition events. It is seen that phases shift through events. This is the simplest state machine and is used as the locomotion control scheme for simulation and experiment mentioned in the coming chapters.

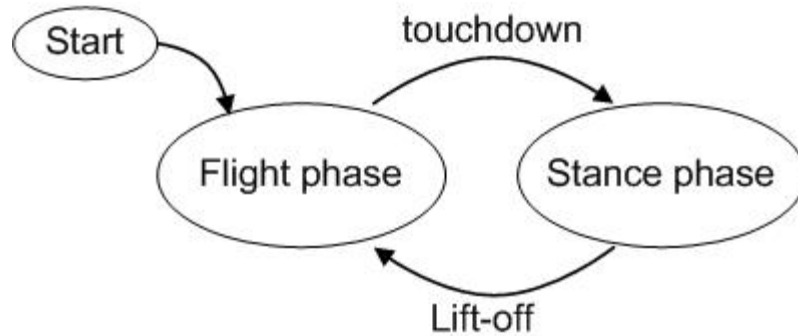


Figure 3. Cycle of the two phases with the two phase transition events

2-3-1-2. States

Aside from the phases, designers should define *states* in order to determine the condition of a legged robot as they keep in mind that states are not separate from dynamical characteristics. Designers usually assign one control method in one defined state so that states can be directly exploited in a total locomotion controller. Designers should make sure that *events* that divide those states are clearly defined along the definitions of states. An event is often used to know the timing for switching control methods, and therefore, such an event does not necessarily change the robot’s dynamical characteristics. Designers can also use as many states in a controller as they wish. Therefore, running controllers can possess more states than the number of phases.

However, switching control methods causes more complexity in analysis and controller design. It is a good idea to restrict the number of states that designers define. Thus, the author first tries stance and flight phases as states and touchdown and lift-off events as state transition events (From here on in, therefore, “phase” and “state” are equal when the author describes the controller or the condition of the robot.). One control method is used for one state: One control for stance phase in order to retract the leg; Another control for flight phase in order to protract the leg. They are switched soon after an event occurs. This is probably the simplest locomotion controller possible as long as a kind of gaits to move the leg back and forth is adopted.

2-3-1-3. State machine

The *State machine* is the state flow of a locomotion controller that has state conditions divided by discrete events. Usually it is closed as a locomotion cycle. To design a running controller for a hopping robot, states and events must be defined and a state machine diagram must be completed and closed.

In the case of Raibert's work, his robots had five states as shown in Figure 4. His robots basically had two actuators: One for the rotational joint actuation in the hip and the other for the prismatic joint actuation along the leg. In the stance phase, his robots had to detect events for four states in order to control the prismatic actuator. If two actuators have to be operated in five states as for Raibert's robots and if each state requires a different control method for each actuator, there have to be 10 control methods.

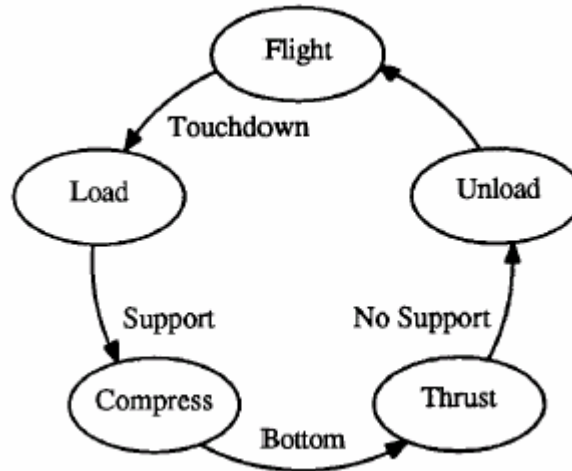


Figure 4. State machine for a planar one-legged hopping robot. The five states are shown along with the events that trigger the state transitions. Reproduced from [32]

The robot in the author's research does not have an actuated prismatic joint in the leg. This is a good thing in terms of power consumption, calculation cost, electrical parts cost, mechanical parts cost, and so on. The mechanical design becomes much

simpler, and the weight is less. The controller can be much simpler. Because one motor is saved by adopting an unactuated prismatic joint, the number of necessary control methods is at most the number of the states only. Since the two phases are chosen as the states of the state machine in the entire controller as in the previous subsection, the running controller consists of stance phase control and flight phase control. These two control methods should be necessary and sufficient, and the controller probably has the simplest state machine.

However, the unactuated joint is not good for everything. The author has to come up with two sets of a flexible control method that can handle one entire phase. One of the hardest parts in controlling the robot by using only one actuator at the hip joint is that there is no thrust input in the prismatic joint in order to obtain a higher hopping height. Only an actuator in the hip joint can be used to increase hopping height. At first glance, it seems that the effect of the hip actuation is coupled in forward direction and vertical direction, i.e. it might be difficult to increase or decrease apex height alone by keeping the same forward speed. If forward and vertical forces can be well distributed between apex height and forward speed, one hip motor could be sufficient enough. The details from an energetic point of view on this distribution issue are discussed in the next subsection and later on.

2-3-1-4. Phase detection

The robot needs a different controller scheme for each phase because the dynamics and associated controllers of each phase is different. Reflex control is used so that the entire locomotion controller can switch control methods at the right moment. Therefore, the controller requires that the robot detect the relatively precise moments at which events occur, i.e. the moments of the phase change at touchdown onto the ground and at lift-off from the ground. In simulation, the leg toe height is measured for that purpose, and in experiment, an infrared distance sensor is attached on the leg toe.

2-3-2. Leg control

The robot knows its phase and controls the leg depending on the phase. (Note that phase can be replaced by state for the description of the author's controller.) In the stance phase, the leg is swept backwards and kicks the ground. In the flight phase, the leg is swung forwards to bring itself to a desired touchdown angle. The author trusts the self-stability property of SLIP [22], [23], [24] and does not make any special effort for stabilization of hopping, but simply sets a leg angle at touchdown and another at lift-off. The touchdown leg angle is imperative for exploiting the self-stability property because it is one of the fixed-point state vector elements. This property is described later in 2-3-2-4. *Stabilization*, and the fixed point is also explained later in 3-2-2-5. *Phase plots and limit cycles*.

2-3-2-1. Leg angles at touchdown and lift-off

Leg angle at touchdown γ^{TD} is 40 *deg* (measured at the hip joint from the vertical line), and leg angle at lift-off γ^{LO} is -25 *deg*. These values have been empirically determined and are fixed in this research. Though those numbers are not yet rigorously derived and proved, there are some reasonable explanations for them. Here the author provides those explanations from physiological and energetic points of view.

2-3-2-1-1. Forward speed and sweeping range

From animal data, 34 *deg* is an average value at a physiologically equivalent speed [14], [16]. It seems that touchdown angles of animals are not dependent on their size (dimension or mass) but on their relative forward speed. It is natural to think that the stride is wider if animals want to run faster, i.e. the wider the running stride is, the faster an animal runs, and vice versa. In fact, the relation has been demonstrated using Planar Biped [43]. An approximate forward speed for the author's SLIP robot is calculated using the equation from [16], which includes a variable touchdown angle:

$$\dot{x} = \frac{2r_0 \sin \gamma^{TD}}{T_s} \quad (13)$$

Where \dot{x} is forward speed, r_0 is rest length of the leg, γ^{TD} is leg angle at touchdown, and T_s is stance duration. The derivation of this equation is based on the assumptions that the leg length does not change throughout the stance phase and that the lift-off angle is same as the touchdown angle (geometrical symmetry).

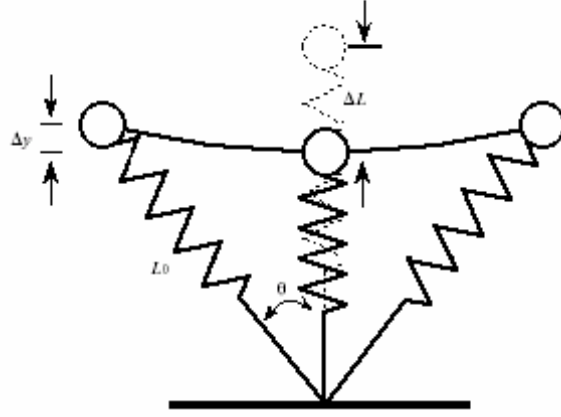


Figure 5. SLIP model in stance phase [16]

Transforming Eq. (13) for the touchdown angle,

$$\gamma^{TD} = \sin^{-1} \left(\frac{\dot{x} T_s}{2r_0} \right) \quad (14)$$

By inspection of Eq. (14), the touchdown angle is dependent on the forward speed, the stance duration, and the rest leg length. Forward speed is variable because it is a matter of control, but the other two are not variable under the assumption for the formula because those values are from mechanical characteristics and structures. Thus, Eq. (14) indicates that roughly speaking, the touchdown leg angle is exclusively dependent on the

desired forward speed. This indication agrees with the common sense that the faster an animal runs, the wider its running stride is (Of course, there are limits to this.). Based on the equation, a plot for touchdown leg angle versus desired forward speed is obtained as in Figure 6. Though it is a function of arcsine, in the region of interest it is almost linear and therefore, the correspondence between the two is clear.

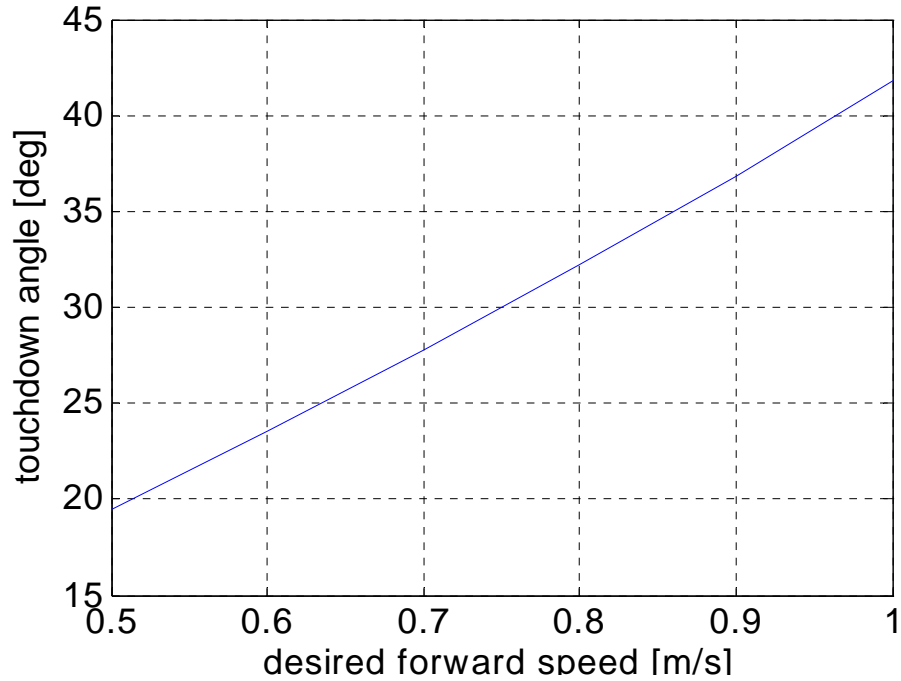


Figure 6. Touchdown leg angle vs. desired forward speed for $m=0.54\text{ kg}$, $k=193\text{ N/m}$, $r_0=0.120\text{ m}$

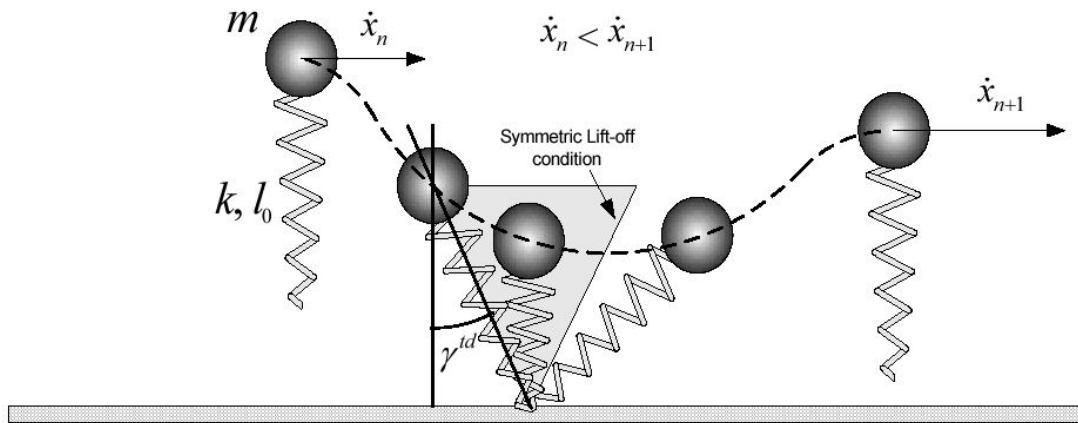
The chosen value for the desired forward speed is 0.8 m/s because the touchdown angle corresponding to 0.8 m/s in Figure 6 is 32.3 deg and is close to the average animal value of 34 deg . The lift-off angle should be approximately -32.3 deg due to the time-reversing/geometrically symmetrical property [45]. Consequently, the sweeping angle is twice as wide as is the touchdown angle, which is approximately 65 deg .

2-3-2-1-2. Sweeping mid-angle

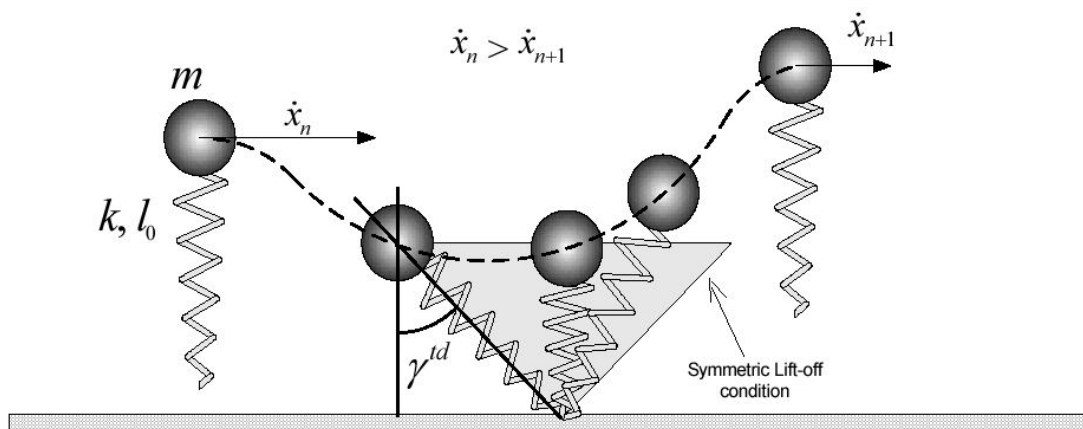
Though the derived sweep angle 65 deg is used, the symmetry property between touchdown and liftoff is not. While the sweeping angle range is kept, the mean angle of touchdown angle and lift-off angle (or *sweeping mid-angle*) is shifted from the vertical line to a certain positive angle in the controller being used. The shifted amount is obtained from trials and errors, based on the desire to maintain stable forward motion.

The reason why the sweeping range is shifted is that hip torque can compensate more in vertical position and speed. Vertical position and speed would be dissipated in an actual robot if the symmetrical gait was used and there were no torque input to the system. This results in lower hopping height after every hopping cycle. To keep a desired hopping height and to maintain hopping cycles, the robot in stance phase needs energy compensation in potential energy or vertical kinetic energy from hip torque. To this end, the reaction force created from the hip torque has to have a sufficient upward vertical element so that the level of vertical position and speed at lift-off are maintained. If the operating range of swept angle was very small and near the vertical line, it would not create a big vertical element in the reaction force. Instead, the operating range should be wide and hip torque should exert torque between the touchdown angle and the vertical angle so that the COM of the body will be pushed more upwards than forwards as in Figure 7(b).

Note that the spring force in the leg is assumed to be an internal conservative force and does not do any work in terms of energy injection. Gravity does not help either since it is a field force for potential energy.



(a)



(b)

Figure 7. Two cases of the hip torque contribution: (a). the most input force directs forwards due to a wide leg angle at lift-off, (b). the most input force directs upwards due to a narrow leg angle at lift-off
 Reproduced from [15]

2-3-2-1-3. Tuning of touchdown, lift-off, and sweeping mid-angles

The shifted amount of the mean angle is experimentally adjusted in such a way that one apex height becomes the almost same height as the previous apex height. One suggested method to adjust it is such that the following two values become more or less the same:

- Vertical distance between a free-fall height and the following apex height, without any energy input
- Vertical distance between the height at a touchdown and the one at the following lift-off.

The touchdown angle is shifted to 40 deg in the case of this research, and as a result, the lift-off angle is -25 deg and the bias of the sweeping mid-angle from the vertical line is 7.5 deg . Note that the shifted amount of the mean angle would be a different value for another hopping robot if mechanical structures were different and the amount of the dissipation energy in a hopping cycle were different.

2-3-2-1-4. Energy distribution

The bias on the mid-point of the sweep angle does not only make it possible for hip torque to maintain a desired hopping height, even without thrust forcing in the prismatic joint, but is also vital for the distribution of mechanical energy.

The total mechanical energy of a SLIP model consists of gravitational potential energy, elastic potential energy, horizontal kinetic energy, and vertical kinetic energy. The ratio of those energy values is maintained at each point, in every hopping cycle, while cyclic hopping is achieved. It comes to the question what happens to the energy distribution when the mean angle of the sweeping range is biased. In the case of vertical hopping, there is no bias since there is no sweeping motion. The kinetic energy at lift-off is the same as the one at touchdown, and the potential energy at lift-off is also the same as that at touchdown. However, in the case of planar hopping, kinetic energy can convert itself into potential energy and vice versa. The balance of the energy distribution can collapse easily. Hence, the control and maintenance of the energy balance is one of the key points for stable, cyclic hopping. From this point of view, the author looks at four issues on the relation between the sweeping bias and the energy distribution as follows:

- The total kinetic energy at lift-off is smaller than that at touchdown
- The gravitational potential energy at lift-off is bigger than that at touchdown
- Part of the forward speed at touchdown is converted to the vertical speed at lift-off
- The sum of the kinetic energy and the gravitational potential energy is same at touchdown and lift-off, assuming the energy input and loss throughout stance phase are well balanced at steady state.

The first statement mentioned is about that energy conversion from kinetic energy to gravitational potential energy, which is caused by the bias of the mid-point of the sweep angle. In order for hopping motion to be cyclically stable, the total mechanical energy should be well balanced. To be like that, the kinetic energy should decrease from touchdown to lift-off by the difference between the two gravitational potential energy values at touchdown and lift-off. If it is achieved, the sum of the kinetic energy and the gravitational potential energy is the same at touchdown and at lift-off.

The event in the second statement is the same one as in the first statement. The absolute value of the touchdown angle is wider than that of the lift-off angle. A wide touchdown angle means that the touchdown height is low, and a narrow lift-off angle means that the lift-off height is high. The gravitational potential energy increases from a touchdown to the following lift-off.

The third statement is about the distribution of kinetic energy. Because of the narrow lift-off angle, the spring's bouncing motion contributes to the restoration of the vertical element in velocity rather than to that of the forward element. Therefore, the forward speed at touchdown is converted to the vertical speed at lift-off.

The fourth statement is validated by the experimental results of this research. The successful cyclic motion indicates that the total mechanical energy is well maintained at a certain level in the dynamical system.

2-3-2-2. Forward speed

The author would like to obtain the highest possible hopping speed, and, for that reason, a relatively high forward speed 0.80 m/s is used in the earlier section. This value might perhaps not be the maximum value the robot could achieve. The reason is that the experimental results for the current and torque-speed curve of the motor (in Figures 35 and 36 shown in Chapter 6) prove that the actual motor rotation is not completely saturated. A faster speed and a longer maximum torque can be provided for a wider touchdown angle and a stronger acceleration. Once the robot reaches a steady state, it will not need so much energy input even at a high speed.

In this research, however, the author sticks to use 0.80 m/s , and other possibilities are to be investigated in future work. It would be necessary to use different PD control gains for different desired forward speeds in order to implement good follow-through motion as described in 2-3-2-5-6. *Adjustable response shape*. That would make analysis more complicated. Thus, to keep it simple and to see the essential points, it is important to use only one case of the desired forward speed.

For reference, TABLE III shows approximate leg lengths, speeds, and dimension-less speeds of the machines that have been used to study the control of legged locomotion. Data for RHex (tripod gait) are from [35], for Scout II from [36], for RHex (bounding gait) from [37], for Planar one-leg hopper from [38], for Monopod from [32], for Monopod I from [39], for Monopod II from [40], for Bow leg hopper from [41], for Pneumatic monopod from [42]. The rest are all from [43]. Note that only Planar Biped, RHex with an optimized tripod gait and Pneumatic monopod have been explicitly designed for high speed.

If 0.80 m/s is achieved, it is already a good achievement by itself. If it is considered in the *dimension-less speed* [44], [45] (the speed value divided by the leg

length), the robot's forward speed is very high. In other words, the dimension-less forward speed is very fast. Note that it is called the dimension-less speed owing to the dimension-less analysis method in [44] and [45], although it has a dimension of 1/s.

$$\hat{x} = \frac{\dot{x}}{r_0} = \frac{0.80}{0.120} (1/s) = 6.7 (\text{leg length} / s) \quad (15)$$

The robot can travel at a distance of 6.7 times the leg length in one second. It is the fastest in terms of dimension-less speed compared to well-known one-legged robots in TABLE III. It is even close to Planar Biped's 7.0 1/s [43], which is the fastest dimension-less speed among the bipeds, as shown in TABLE III. A bipedal robot generally can be a lot faster than a one-legged robot with the same leg system because its swing leg can be protracted in stance phase and its flight duration can be shortened so that it can propel itself more frequently. Considering that Planar Biped is a bipedal running robot and uses hydraulic actuators and a pneumatic actuator, the author's SLIP hopper with a DC motor is still very good in speed.

Even compared to the values of animals are in TABLE II in 2-2-2. *Leg spring stiffness*, the author's SLIP hopper is fast. Interesting is the result that the same kind of leaping locomotion as in red kangaroos gives close speeds in dimension-less speed.

TABLE III. APPROXIMATE LEG LENGTHS, SPEEDS, AND DIMENSION-LESS SPEEDS OF LEGGED ROBOTS.

# of legs	Machine	Researcher	Leg length	Forward speed	Dimension-less speed
			<i>m</i>	<i>m/s</i>	<i>l/s</i>
6	OSU Hexapod	McGhee	0.8	0.3	0.4
	USSR Hexapod	Gurfinkle	0.35	0.1	0.3
	SSA Hexapod	Sutherland	1.0	0.14	0.14
	ODEX	Odetics	1.3	0.5	0.4
	ASV	Waldron	1.90	2.2	1.2
	RHex (tripod gait)	Koditschek	0.17	2.7	15.9
4	PV II	Hirose	0.87	0.5	1.1
	Quadruped	Raibert	0.66	3.0	4.5
	Scout II	Poulakakis	0.31	1.3	4.2
	RHex (bounding gait)	Campbell	0.17	1.5	8.8
2	WL10-RD	Kato	0.96	0.23	0.2
	Biper-3	Miura	0.20	0.02	0.1
	Meg-2	Funabashi	0.48	0.5	1.0
	Kenkyaku	Furusho	0.72	0.8	1.1
	Planar Biped	Koechling	0.844	5.9	7.0
1	Planar one-leg hopper	Raibert	0.50	1.2	2.4
	Monopod	Raibert	0.74	2.3	3.1
	Monopod I	Gregorio	0.70	1.2	1.7
	Monopod II	Ahmadi	0.70	2.0	2.8
	Bow leg hopper	Brown	0.25	1.0	4.0
	Pneumatic monopod	Harbick	0.285	1.8	6.3
	SLIP hopper	Sato	0.120	0.80	6.7

2-3-2-3. Apex height

Apex is the vertically highest point at which the robot is in the air. The height at apex is commonly called hopping height. The desired apex height for every hopping cycle is set to be at 0.170 *m*. As discussed in the design subsection for leg length, the desired height should be achieved mainly by the characteristics of the designed mechanical parameters. The sweeping mid-angle and PD gains of motor control are tuned to follow the design, but no other control effort is specified for the desired height. Simple evaluations are done in simulation and experimental results. The controllability for variable height is left for future work.

2-3-2-4. Stabilization

The ideal SLIP model has a self-stability property discussed in [22], [23], and [24], and relevant work on different dynamics models is [25] and [46]. The SLIP model without any energy input is energy conservative, and thus, its motion is an issue for the property. One condition for the self-stability is an appropriate leg angle at touchdown, and it should be assumed that the hip torque to protract the leg to the angle in flight phase does not inject any energy to the system. If the condition is satisfied, then the leg in stance phase is naturally swept to its appropriate lift-off leg angle, its state vector at apex is always the same, and its motion of the SLIP model in stance phase is symmetric in terms of the path in the sagittal plane and time. The path of the COM is symmetric with respect to the vertical line (i.e. the absolute values of its touchdown leg angle and its lift-off leg angle are the same) and the motion is the same if it is followed in a time-reversing manner. This symmetry property is discussed in [47], [48], [49], and [45], and the general symmetry of dynamics is discussed in [50].

No experimental robot can use the hypothesis that it is a conservative system, though it seems that only touchdown angle should be controlled and hip torque in flight phase can be used since the pitch motion of the author's SLIP hopper is constrained (explained in Chapter 5). Therefore, hip torque in stance phase should be exerted on the ground and be used for injecting energy to the system, and the input energy should balance with the dissipated energy.

In terms of energetic stability, hip torque has to input as much energy into the robot during stance phase as the robot loses in one hopping cycle. It is assumed that in the SLIP model, the leg does not have any mass. The author's actual robot is designed in such a way that the mass of the leg is small compared to the body part and can be neglected as well. Therefore, once the robot is off the ground, it cannot inject energy into the whole dynamical system even if the leg is swung back and forth many times; nor can the robot control the balance of kinetic energy and potential energy once in the air. Therefore, the robot has the chance to stabilize its energy only in stance phase, i.e. the control effort to maintain mechanical energy has to be made during stance phase.

In terms of postural stability, the toe clearance from the ground is the important point on continuous hopping. The attitude of the body is not a problem since the body of a SLIP is a point mass and does not have inertia moment nor pitch motion. Thus, compensating mechanical energy in vertical element helps both energetic stability and postural stability at the same time.

2-3-2-5. Control scheme

In this section, the hopping controller is described. It is assumed that the hip actuator is a DC motor. The details on the motor are explained in *Chapter 5: Experimental setup*.

2-3-2-5-1. Overview

The entire controller is composed of two sets of PD control parts. A set of PD control is used to control leg angle using hip torque for the leg sweeping in stance phase and the other set is for the leg swinging in flight phase. The combination of step input and PD control is used to control the leg angle. The desired angle for a state of the robot is commanded depending on which phase condition the robot is in. As soon as the touchdown sensor detects the ground, the stance-phase control part becomes effective. In stance phase, the controller commands a step input of lift-off angle into PD control part and outputs the desired torque in real-time. Similarly, the flight-phase control part is turned on as soon as the ground detection turns off.

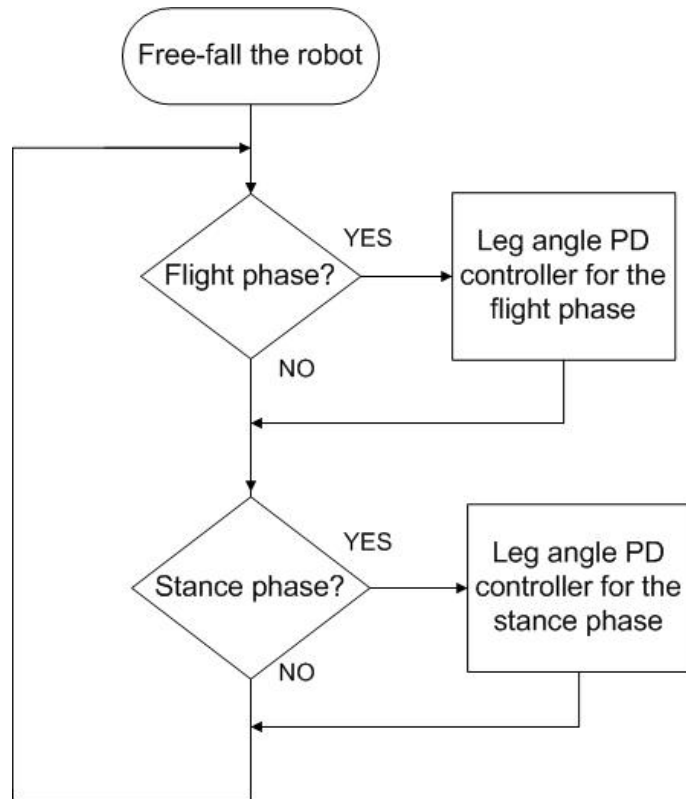


Figure 8. Flowchart of the author's entire control scheme

This alternate use of two sets of PD control is adopted because of the following advantageous features:

- Compatible with reflex control and step input
- Appropriate and easy for angle control
- Stiff (i.e. high torque) when far from set point
- Damped (i.e. low torque) when close to set point
- Having spring-like response coming from the overshoot of the 2nd-order system
- Adjustable amount of the overshoot.

The listed features are discussed one by one next.

2-3-2-5-2. Reflex control and step input

Firstly, commanding a step input to angle PD control by reflex is the main control scheme. Changing controllers by reflex depending on the phase is necessary since each phase's dynamics is totally different. A proper controller has to be applied to the phase that the robot is in, and the lag of shifting to the right controller is likely to cause instability. On the contrary, it can also be said that reflex might be sufficient. One example of reflex control is in Berkemeier's *et al* paper on vertical hopping [44]. Their results show that reflex control with a constant value of step thrust input is simple, applicable, and robust in vertical hopping. Their reflex control is more robust than their periodic forcing input. Furthermore, despite the fact that there is no adaptive change in the constant thrust input by reflex, their reflex control results in being nearly as robust as is their adaptively adjusted thrust input. Also, reflex control for control phase shifting with adaptive feedback has successfully been implemented in all of Raibert's hopping robots [16]. The role of reflexes and the timing for shifting controllers in dynamical legged locomotion are discussed in [56].

The adaptive derivation of a set angle for every single phase is not required for the author's robot. In fact, deriving an adaptive desired angle in every cycle is sometimes a big hurdle for real-time motion control of an autonomous robot owing to its calculation speed. Adaptively deriving a 3rd-order trajectory, for instance, is even worse. It also requires PD high gains in order for the actual leg angle to track a desired angle trajectory, which is not practical for an inexpensive platform. That is why step inputs of fixed angles are used. Note that the actual leg angle in flight phase becomes similar to a 3rd-order trajectory using a step input and it is discussed later in this chapter and in experimental results.

2-3-2-5-3. Angle control

Secondly, PD control is one of the most popular methods to control angle using a DC motor. It is appropriate for a DC motor. Desired angles are easily achieved if a small steady-state error is not a problem. Since the touchdown angle of the leg is one of the conditions for the self-stability property of the SLIP model, angle control is required.

2-3-2-5-4. Stance torque

PD control moves the leg strong and fast, i.e. proportional term governs hip torque, when the leg is far from the set point. Then, it slows down, i.e. derivative term dominates hip torque, when the leg angle comes close to the set point. It is good to have stiff torque of proportional control term from touchdown to mid-stance.

During stance phase, kicking the ground using hip torque creates a force which propels the robot body to the direction perpendicular to the leg. Because of a large touchdown angle, the robot body gains more upward kinetic energy than it naturally would without torque in addition to the forward component of kinetic energy. Also, more gravitational potential energy is injected since the force does work when the robot body is moved to a higher position.

At the same time, the leg spring stores elastic potential energy because the spring is compressed. However, no more elastic energy is stored than there would be without hip torque. The spring force is a conservative internal force. The hip torque does not do any work since there is no force element from hip torque in the direction of the spring axis.

2-3-2-5-5. Spring-like response

The response of a torsional spring at the hip joint makes an energy-efficient leg trajectory. It works with the simulation of a running biped [25] and the simulation and experiment of a hopping monopod [26]. This fact also supports the use of PD control

since one could think that the proportional control term produces an artificial spring response for the leg trajectory.

2-3-2-5-6. Adjustable response shape

Lastly, a property of PD control is one of the decisive advantages. In general, PD control has been widely used because each term of P control and D control has a decoupled role and because gains are independently adjustable. As mentioned before, the proportional control term can adjust “stiffness,” while the derivative term has a strong relation with damping and has control over the amount of overshoot. This controllability of stiffness and damping is useful and makes it possible to have a trajectory similar to a 3rd-order one.

A sine curve of a pendulum with a spring at the pivot in the horizontal level can be approximated by a linear line and a 3rd-order curve. Then, the ideal spring response can approximately be realized by a linear-like trajectory in stance phase and a 3rd-order-like trajectory in flight phase. This concept can be applied to a robot leg, and thus, the stiffness and damping of the leg motion is relatively easy to adjust. This creates the follow-through motion of the leg just after lift-off and the draw-down motion of the leg just before touchdown.

2-3-2-5-7. Comparison to Raibert’s three-part controller

Raibert’s running controller has three parts and each part plays a specified role [16]. The forward speed control part produces a desired touchdown angle in each cycle. The pitch angle control part outputs torque to right up the robot body in stance phase. The hopping height control part determines the amount of thrust force that is applied using a 2nd actuator when the COM is at the lowest point in stance phase.

Inside the author’s simple controller, all the three components in Raibert’s running controller are contained by exploiting the combination of the two PD control parts and the SLIP model; though there is only one actuator. Desired forward speed is

fixed and therefore, desired touchdown angle is constant. The COM is considered using the SLIP model, and therefore, pitch angle is not taken into account. The hopping height is to be achieved by empirically tuning the sweeping mid-angle.

Chapter 3: Simulation implementation

The robot is an event-driven, intermittent dynamical system, and therefore it is often the case that, for analysis, analytical solutions are difficult to obtain and numerical simulation is the means to a solution. Numerical simulation is done in order to investigate the possibility of the realization of a Spring Loaded Inverted Pendulum (SLIP) and its stable hopping.

The author has the mechanical parameters for a SLIP and a controller for it, and therefore, he has the necessary information for simulation. They are implemented in simulation using the Matlab and Simulink software packages [57].

3-1. Dynamics Models

Approximate models for stance and flight phases are used while the essential characteristics of the SLIP model are preserved: A ballistic flight model and a planar harmonic stance model.

In the flight phase, it is assumed that the center of mass (COM) flies along a ballistic trajectory since the COM is a point mass and the mass of the leg is included in

the mass of the body. In the flight phase, however, the inertia of the leg is still taken into account in order to calculate the effect of hip torque on leg motion. The motion of the COM and that of the leg are considered to be able to be decoupled.

In the stance phase, the SLIP is represented as a harmonic system in the sagittal plane. The inertia of the leg is neglected. Ground contact between the toe and the ground is modeled as a pin joint so that the toe does not slip on the ground surface. Friction of the joint is neglected.

The effect of impact at touchdown and lift-off is neglected as well though there is impact between the toe and the ground and there is impact between the prismatic joint slider and the mechanical stop of the prismatic joint on the actual robot which is mentioned later.

The equations of motion are obtained for each phase model using the Lagrangian Methodology [58]. For the flight phase,

$$\begin{aligned}
 \ddot{z} &= -g \\
 \ddot{x} &= 0 \\
 \ddot{\gamma} &= -\frac{\tau}{J_{leg}}.
 \end{aligned} \tag{16}$$

For the stance phase,

$$\begin{aligned}
 \ddot{r} &= r\dot{\gamma}^2 - g \cos \gamma + \frac{k(r_{rest} + \delta - r)}{m} - b\dot{r} \\
 \ddot{\gamma} &= -\frac{2\dot{r}\dot{\gamma}}{r} + \frac{g \sin \gamma}{r} - \frac{\tau}{mr^2}.
 \end{aligned} \tag{17}$$

where r is leg length, δ is pre-deflection of the spring, τ_h is hip torque, z is vertical position, x is horizontal position, and the parameter values in simulation including motor and gear parameter values are as in TABLE IV.

A motor and gear model is added in the simulation. In order to have a realistic result, the maximum current that can be input into the motor is limited at 5 A. It is imperative to limit the available torque at the hip joint based on the performance of the motors used on actual robots [27], [19]. The available hip torque of the SLIP is within a torque-speed performance curve, and it is implemented in simulation. A torque-speed curve on experiment is plotted in Figure 36 in Chapter 6. For details, refer to [27] and [19]. For a point of view on the general dynamics and control of systems with saturated feedback, [59] and [60] might be interesting.

TABLE IV. PARAMETERS FOR DYNAMICS MODELS

Parameters	Symbols	Values	Units
Body mass	m	0.540	kg
Spring constant	k	193	N/m
Rest leg length	r_0	0.120	m
Pre-deflection	δ	0.024	m
Leg damping constant	b	0.35	$N s/m$
Leg inertia	J_{leg}	2.0×10^{-4}	$kg m^2$
Gravity acceleration	g	9.805	m/s^2
Stall torque	τ_{stall}	0.081	$N m$
No-load speed	ω_{nl}	3380	rad/s
Torque at current limit	τ_{cl}	0.020	$N m$
Total gear ratio	R	173	-
Torque transmission %	T	0.90^4	$10^{-2} \%$

3-2. Methods

3-2-1. Numerical simulation settings

The simulation is done using the Matlab and Simulink software packages [57]. The adopted integrator is a 4th-order integrator using Runge-Kutta method. Variable step time is used for the integration. The maximum step size and the tolerance are of both $1 \times 10^{-3} s$.

3-2-2. Stability analysis

It is essential to have a measurement standard to evaluate whether the designed robot is capable of running in the desired fashion. Simulation and experimental results are to be accessed by the standard and related ideas for stability.

3-2-2-1. Analysis tool selection

Raibert's three-part controller [16] has been used by many researchers for two decades and researchers, to some degree, have been satisfied with the control method. On the other hand, researchers still seek measurement standards for the stability of legged running and some have used the following tools:

- Phase plots by Michalska *et al* [61]
- La Salle's theorem by Ahmadi [26]
- Regions of attraction by Schwind *et al* [62]
- Return maps and fixed points by Koditschek *et al* [62], [45].

For the author's analysis, stability analysis tools should be compatible with both simulation data and experiment data. Accordingly, the author uses phase plots and regions of attraction. The phase plot is adopted as it is. Some ideas are added to the

region of attraction. Moderate stability definitions are utilized in order to make the analysis realistic and usable for experimental data with errors.

La Salle's theorem is an analytical material and it is not proper for experimental data of the SLIP hopper.

Fixed points are not directly used. Intermittent and nonlinear dynamics has been preventing researchers from investigating the stability of legged robots by using traditional methods for usual continuous or discrete systems. For instance, verifying only the sign or magnitude of the eigenvalues of the system matrix in a state-space representation is not useful. Those systems must be treated differently from ordinary systems according to Guckenheimer and Holmes's work [63]. That is why Koditschek analyzes the stability of the SLIP model of a hexapod robot called RHex by the numerically computed determinant of the return map Jacobian or the determinant of the numerically determined fixed points [45]. Unfortunately, it is not realistic to directly apply their tools to experimental results. Consequently, the author utilizes the other methods in the following sections.

3-2-2-2. Stability definition

In the author's research, to simplify stability analysis of empirical data, *stability* is fundamentally defined as follows:

- **Ability or condition for the robot system to converge into a steady state and run continuously.**

Based on this definition, phase plots and transition plots described later are considered.

3-2-2-3. Lenient criteria for convergence

An IC can result in convergence after several hopping cycles even though it does not converge after one cycle only. Hence, it is a good idea to observe several cycles in order to determine if an IC leads to convergence in the end.

Thus, the following two cases are accepted as the IC's that converge:

- An IC converges into a desired condition after several cycles
- An IC does not diverge and stays inside a small area around a desired condition.

These are why accurate fixed points are not specifically obtained in the author's research. Rigorousness is an obstacle though searching for fixed points is one good method to find out stability in numerical simulation. In reality, there are modeling errors, machining errors, mechanical wearing, digital system error, and environmental disturbance. Error must be flexibly allowed in the author's experiment.

3-2-2-4. Robustness

Another issue is that even at a fixed point, it can go off the stable condition because of errors and disturbances. The idea of robustness is introduced and combined. *Robustness* is defined as follows:

- Property to recover to the stable condition once out.

If a robot is robust and a disturbed condition is within a tolerable range, it can regain the stable condition after disturbance.

If many IC's surrounding a desired condition converge into the desired condition, the robot is regarded to be robust, i.e. to be capable of negotiating disturbance. Transition plots are obtained in order to find out robust stability in this sense.

3-2-2-5. Phase plots and limit cycles

In general, a phase plot of *stable* periodic dynamical motion, such as in a robot's hopping, results in a closed periodic orbit [64], [32], [61], [65]. For instance, the characteristics for a phase plot of vertical position versus speed is known for the hypotheses that during flight phase, the COM follows a simple ballistic trajectory under the influence of gravity and that during stance phase, it follows a harmonic trajectory consistent with the simple spring-mass oscillator, and this combination results in a closed orbit. This kind of closed orbit is called a *limit cycle* and is *stable* [66], [67].

Phase plots and transition plots (mentioned in the following section) become abstract in terms of understanding the entire dynamics from solutions. Transition plots lose more information of the systems than phase plots do. However, these methods are recommended in [67], [68], and [69] because they are practical in implementation and useful to find out stability when analytical methods are complicated and difficult.

To investigate stability, a phase plot of vertical position is examined in the simulation results of Chapter 4. Furthermore, phase plots of leg angle and leg length in addition to that of vertical position are discussed in the experimental results of Chapter 6.

To summarize, if the path of a phase plot converges into a limit cycle, the used initial condition and the system are considered to produce *stable* motion in terms of the variable for the phase plot.

3-2-2-6. Transition plots and regions of attraction

Analytical integration of the equations of motion of legged robots is usually not possible owing to their nonlinear and intermittent dynamics. Therefore, mathematical tools compatible with numerical simulation are highly desired. Especially in the author's study of a robot and controller design, numerical simulation is sufficient. Such a tool for understanding the stability of periodic orbits is the *Poincaré map* [63], [70], [71], [72]. It is also called *stride function* [25] or *return map* [73], [45], [62] in legged locomotion. It is a discrete map created from a continuous dynamics or from a combination of several continuous dynamics, and therefore, analysis becomes easier.

Fixed points can be searched for by applying this tool to legged robots. A *fixed point* is a point that is on a cross section (or *Poincaré section*) in a state space and that can return to the exactly same condition after one Poincaré map operation of one locomotion cycle. Hence, once a robot is at a fixed point, it will remain there in a selected section, which can be regarded to be stable and cyclic.

Studied in the author's research are the plots of the sequence of points of return map operations of the state vector (z, \dot{x}) on the 2D- cross section at apex (i.e. highest position in flight) for every cycle. The author calls it a *transition plot*. By obtaining the sequence for enough cycles in a transition plot, convergence and the steady state error for an IC can be checked. Time information is not contained since the state vector does not have time as a state, but it can show convergence speed not per the actual time but per the number of cycles.

In the case of transition plots, if a state of the robot converges into a desired state and it maintains hopping, the robot is regarded to be in a stable condition. All the possible IC's should be examined in order to see the range of IC's that lead to stability. Then, all and only the IC's that converge should be plotted. The domain created by the points is called the *region of attraction* for the robot [62]. Note that, for regions of attraction, the traces of transitions to convergence are not included.

The author's simulation does not plot all of the points that can converge because the IC's reasonable for the mechanical structures of the robot and planarizer are tested and plotted.

In terms of robustness, the larger the region is, the more robust to disturbance the robot is. If a region of attraction is large, the IC can be distant from the center of convergence area. Each IC point can be regarded as the state with error after being disturbed at a steady state. Its plot shows how far the error can be from a steady state and how far in terms of the distance or speed (if the phase plot is of position vs. speed) the robot is able to recover its posture and hopping cycle from.

Chapter 4: Simulation results

The simulation based on the mechanical parameters determined in *Chapter 2: Design* has resulted in stable running. Several plots show the strong possibility of the successful implementation of a Spring Loaded Inverted Pendulum (SLIP) hopping robot.

4-1. Motion in the Sagittal Plane

If the initial condition (IC) is of forward speed 0.80 m/s , vertical position 0.180 m and vertical speed 0 m/s , then the robot smoothly goes into a cyclic motion as shown in Figure 9. The desired state is set to be of forward speed 0.80 m/s and vertical position 0.170 m . The state at the 14th apex (about 5 s) is forward speed 0.63 m/s and vertical position 0.171 m . (Apex is the highest point in flight.) This result indicates that a SLIP robot using only one actuator with the limited motor performance is feasible.

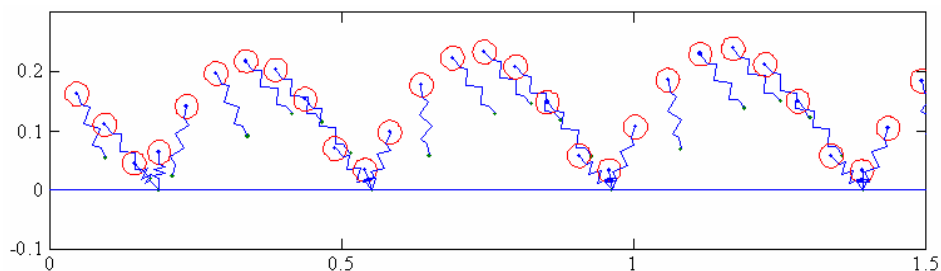


Figure 9. Hopping motion in the Sagittal Plane

The plot for the position of the center of mass (COM) in the sagittal plane is shown in Figure 10. The IC is of forward speed -0.60 m/s , vertical position 0.260 m , and vertical speed 0 m/s . In spite of the large initial error, the robot recovers its forward speed and adjust its height, and its state converges to the desired state of forward speed 0.80 m/s and vertical position 0.170 m .

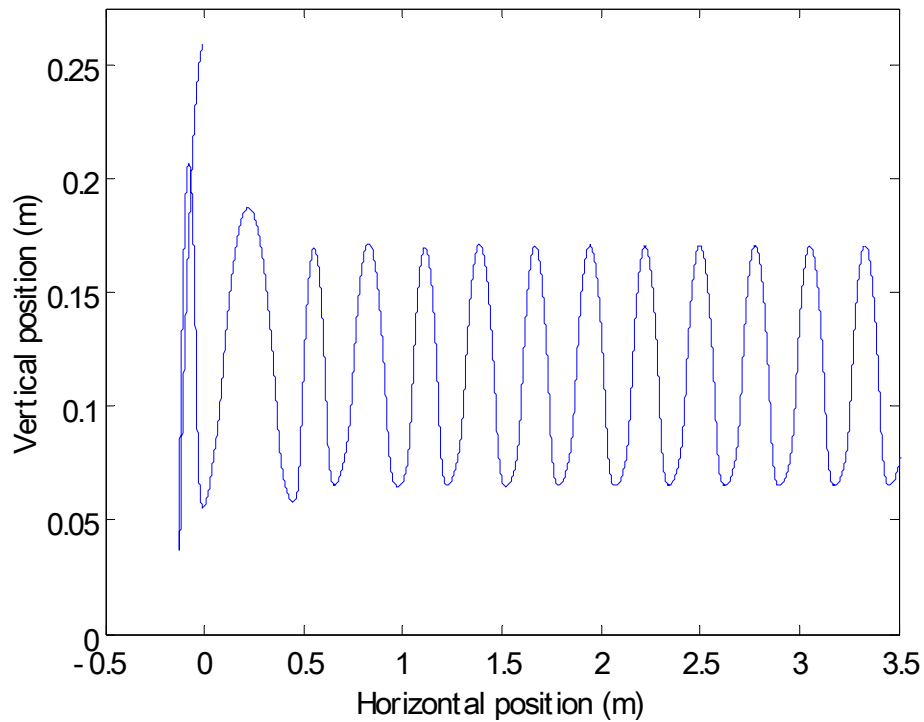


Figure 10. Position of the COM in the sagittal plane.

4-2. Phase Plot

The phase plot for vertical position of the center of mass (COM), i.e. vertical speed versus vertical position, is shown in Figure 10. The IC is forward speed -0.60 m/s , vertical position 0.260 m , and vertical speed 0 m/s . The plot turns out to be a closed orbit, i.e. a limit cycle. One round designates one hopping cycle, and therefore, hopping height converges quickly and is cyclic and stable. The approximate apex height in Figure 10 shows that the toe clearance is about 0.050 m since the leg length in the flight phase is 0.120 m .

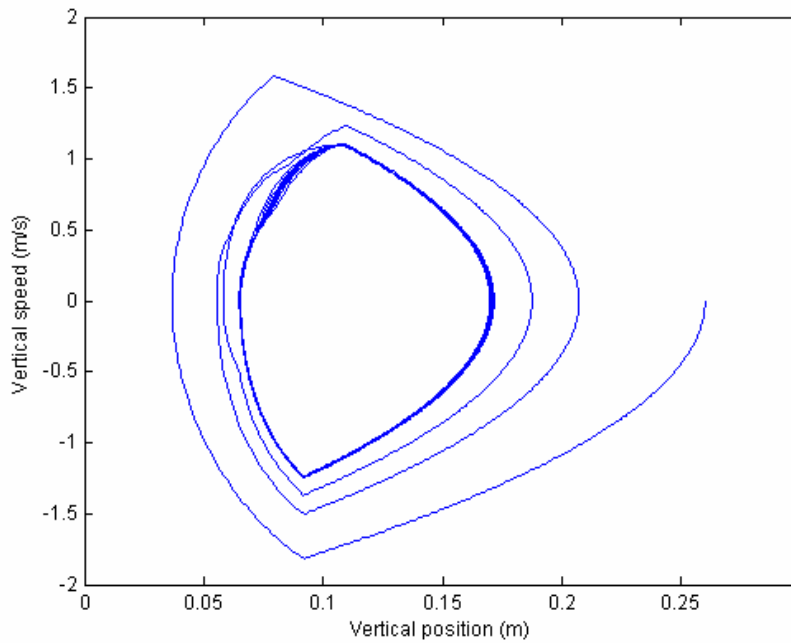


Figure 11. Phase plot for the vertical position of the COM

Using the same data set, vertical position-speed trajectory is plotted in 3D in Figure 12. This is a plot of vertical speed versus position with time. It results in a helix-like spiral, and the convergence with respect to time is seen because the radius of the spiral becomes smaller as the time progresses.

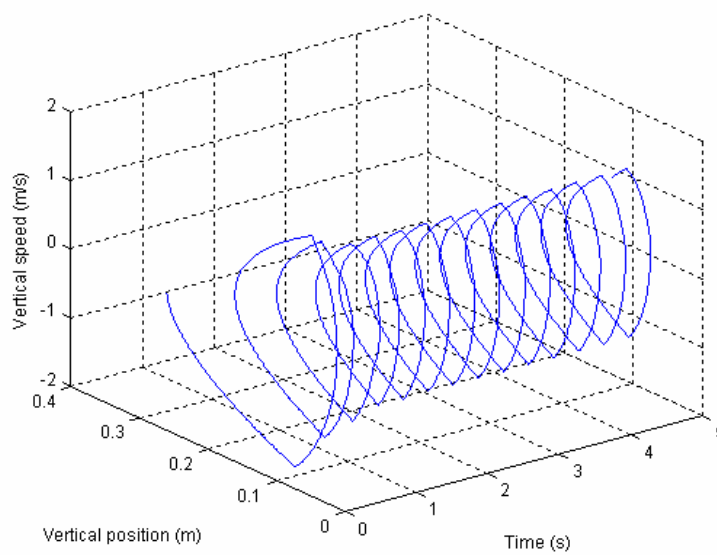


Figure 12. Vertical position and speed trajectory

4-3. Transition plot and Region of Attraction

Figure 12 shows how one IC converges into a stable state. The same IC is used as for Figure 10. The state at every apex is logged and plotted so that the transition can be seen.

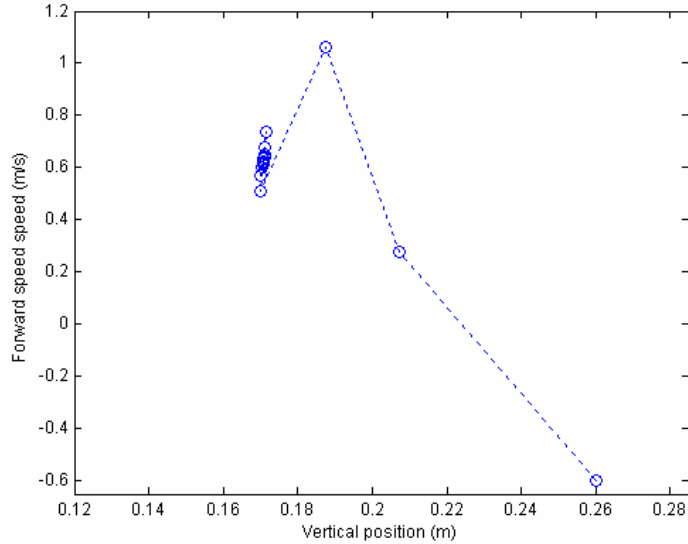


Figure 13. Convergence transition

The author has tried 2115 points as IC's in order to obtain a region of attraction as shown in Figure 13. It does not have traces of transitions. Two solid lines are drawn at 0.170 m and 0.8 m/s . A circle dot (\bullet) means that the IC point converges into the desired area of apex height between 0.169 and 0.173 m and apex forward speed between 0.61 and 0.65 m . This height range is as desired. This forward speed range is lower than desired but results in approximately 0.8 m/s when averaging of the whole cycle. This is due to the forward speed in the stance phase, which is faster than 0.8 m/s . A plus mark ($+$) means that the leg length is shorter than 0.030 m at some point in 5 s , though the leg length does not become 0 m and the point converges into the desired area. These values come from the physical limit of the actual robot structure. A cross mark (\times) means that the IC does not converge into the desired area.

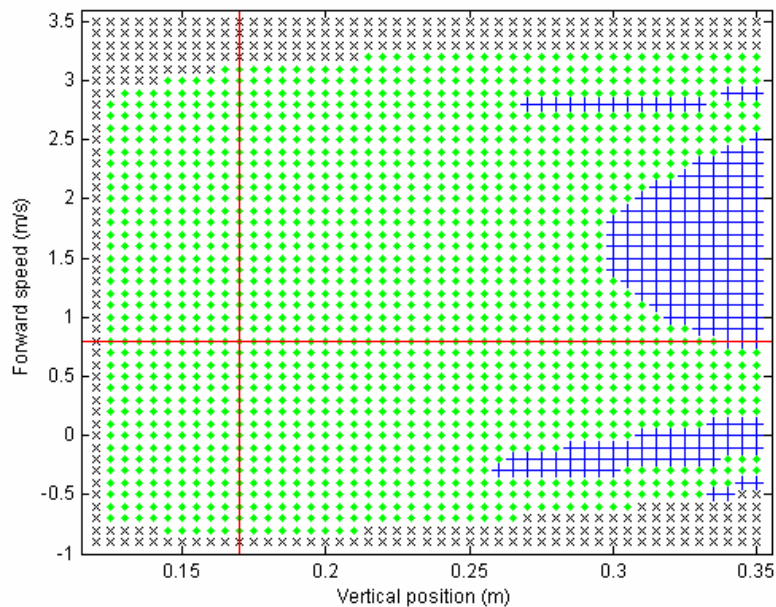


Figure 14. Region of attraction in simulation

It is seen that the IC's in a large domain even with such a large error as negative forward speed -0.5 m/s converge into a cyclic hopping. Thus, a small disturbance from the actual environment will not prevent cyclic hopping motion, and this indicates that the SLIP can be realized.

4-4. Summary

From the simulation results, the following conclusions may be led:

- Only one actuator is sufficient to stabilize a planar hopping robot
- A servo system with one DC motor is strong enough to stabilize a planar hopping robot
- A simple PD controller is sufficient to create a stable running motion and sustain it for at least 5 s.

The possibility to realize a SLIP is confirmed in the simulation.

Chapter 5: Experimental setup

In this chapter, the details of experimental setup are mentioned. First, the mechanical structure of the robot and the planarizer used is described. Then, the computer and electronic system structure of the entire setup is described. Lastly, the different point of the experimental method from the simulation is explained.

5-1. Mechanical Structure

5-1-1. Overview

The three parameters in Chapter 2 are taken from the values designed for building a Spring Loaded Inverted Pendulum (SLIP) robot. Figure 14 shows the CAD design of the robot with a planarizer. The planarizer consists of two beams and a rotation base, which is needed for approximating sagittal plane motion. It constrains the pitch motion of the robot in order to conceptually place the center of mass (COM) of the body at the hip joint axis. Figure 15 shows the entire view of the actual setup of the robot with a planarizer. Figure 16 shows a close view of the robot. The springy leg is realized as a compliant, passive prismatic joint. The lower leg shaft slides along in the upper leg, inside of which there are linear bearings. There is only one actuated DOF at the hip. There is one motor with 4-stage gears and a potentiometer in the black servo

casing behind the white upper leg bushing. On top, an aluminum block is attached. Sensors are on the robot and the planarizer. Sensor configuration can be checked from an electronic system point of view in Figure 18 of the next section.

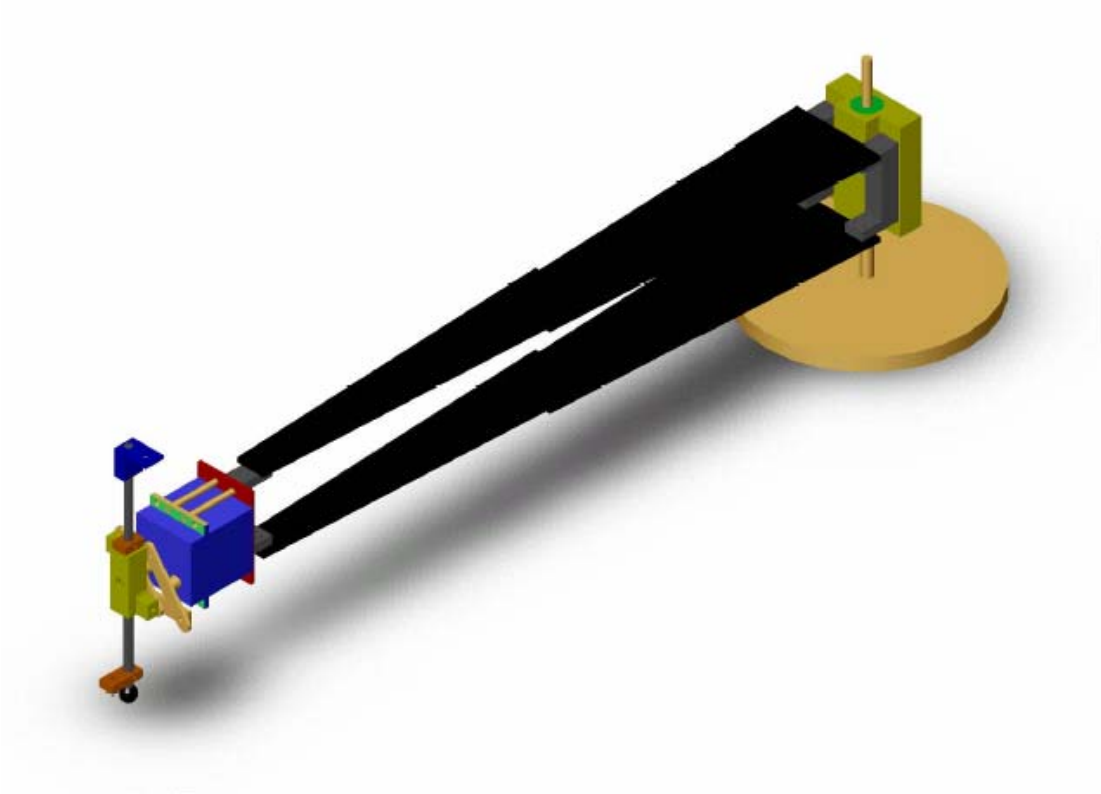


Figure 15. Entire view of the CAD design of the robot with a planarizer

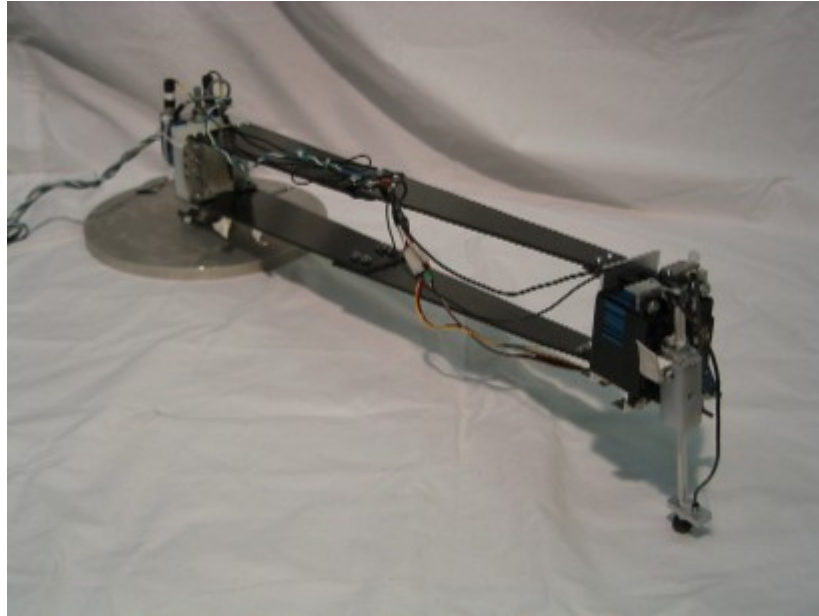


Figure 16. Entire view of the actual robot and planarizer with a planarizer

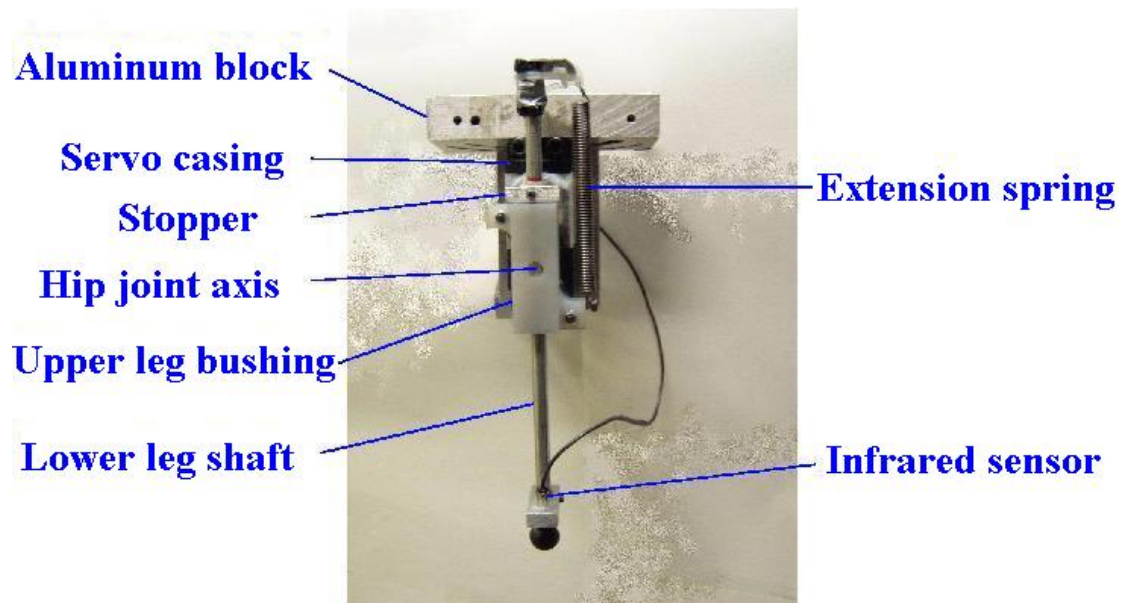


Figure 17. Close view of the robot

5-1-2. Planarizer

In general, the 2-Dimensional (2D) motion of a non-point object has 3 Degrees of Freedom (DOF) – the horizontal displacement, the vertical displacement, and the pitch angle rotation – while the 2D motion of only a point mass has 2 DOF without the rotation. The author uses x and z for the 2 DOF and γ for the leg angle with respect to the vertical line in order to describe the author's robot.

In the case of the experiment part of this research, the body of the robot represents a point-mass system of Spring Loaded Inverted Pendulum (SLIP) model. SLIP is a point-mass model with a virtual springy leg in the sagittal plane (Please see section 1-1. *Motivation* for descriptions.). A point-mass system requires two coordinates in a plane and no more. Therefore, the body must have only two DOF of motion, and the pitch angle rotation is not desired in the robot's motion. So, the motion of the robot needs to be constrained in a plane and the pitch motion is simultaneously restricted.

A circular boom type as in Figure 17, which is often adopted in legged locomotion [16], [17], [74], is used. The advantage of this type is that the robot can go in circles for a long distance. The author's planarizer has an extra feature of a parallel mechanism of two beams in Figures 14 and 15.

The beam length of the author's planarizer is designed such that the distance between the planarizer center (center of the rotation base) and the leg position will be 0.660 m when the robot is at rest on the ground and the boom is not horizontally inclined. The distance the robot can travel in a circle is $2\pi \times 0.660 = 4.15\text{ m}$, and It takes the robot about 5 s to travel that distance if the robot goes at 0.80 m/s as desired (This desired forward speed is discussed in section 2-3-2-2. *Forward speed*.). The robot hops approximately 13 times in a circle if the stance time is 0.165 s and the flight time is 0.240 s. Therefore, the radius of this planarizer should be large enough to regard it to be a plane constraint.

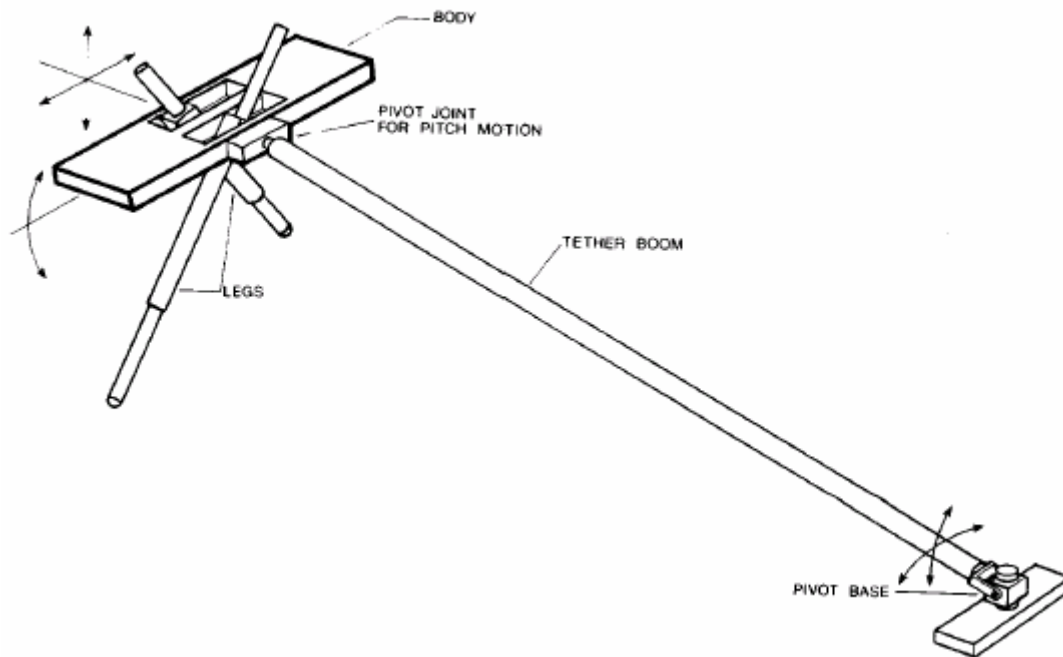


Figure 18. Raibert's circular-boom-type planarizer with 3 DOF for Planar Biped [16]

5-2. Computer & Electronic System

In this section, the system structure is first described. Next, the selection of computer and electronic components for the platform is described. Then, the implementation of controller code is explained.

5-2-1. Structure

Two computers are used: The host computer is used for programming code and the target computer is for running the compiled code in order to control the robot. The sample rate for control is 1 *ms*. The robot is tethered to the target computer. The robot has a potentiometer for hip angle and an infrared sensor for ground detection. Two potentiometers are on the planarizer to measure the position in the constraint plane.

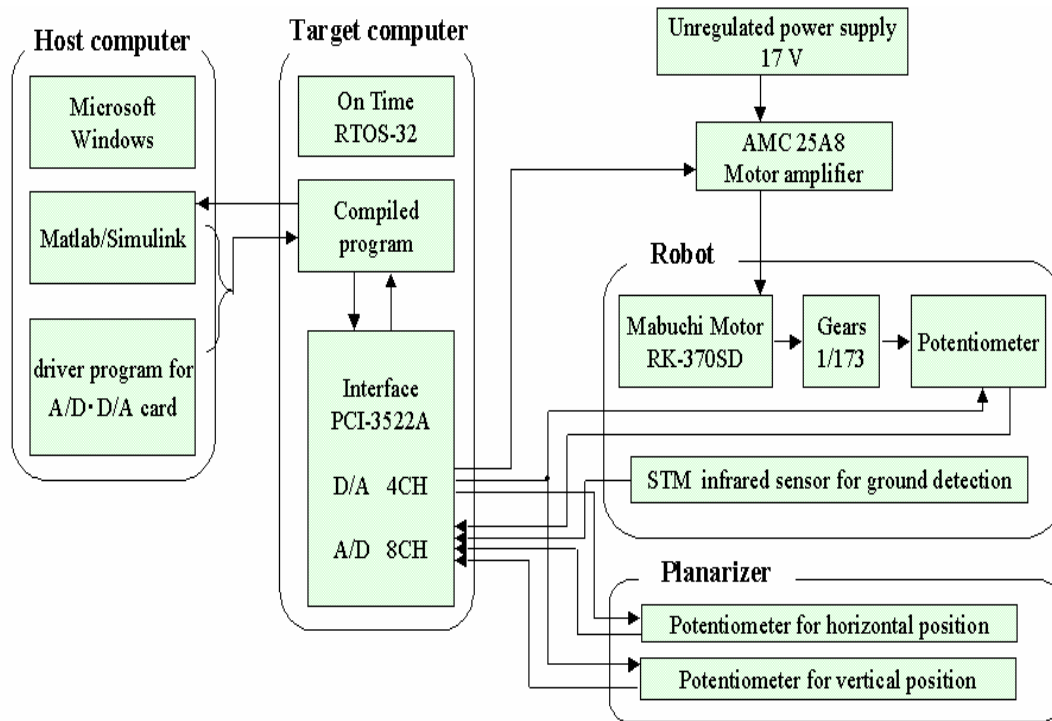


Figure 19. Computer & Electronic System structure

5-2-2. Hardware components

In this section, the author describes the selected components of computer and electronic systems.

5-2-2-1. Computers

Two computers are used. One is used as a host machine in order to code the controlling program for the robot. The other is used as a target machine in order to run the code that is uploaded from the host machine and to control the robot in real-time.

On the author's experimental setup, both are ordinary desktop computers. However, the target computer should ideally be an embedded computer such as a PC104

computer so that the robot can become a power-autonomous robot. The idea that the author uses two computers is for a good platform environment because, with a host, a lot of heavy research work, such as simulation and development, can be done and, with a target, the robot can go on its own in practical environments.

For the two computers to communicate with each other, a Local Area Network (LAN) connection using Ethernet cards is adopted. Ethernet cards are available at any computer stores and inexpensive. The connection speed is quite fast because the communication is used only when the host uploads an executable program to the target and when the host downloads logged measurement data. In addition to that advantage, a LAN connection saves the possibility of using a wireless connection with an autonomously powered system.

5-2-2-2. Operating Systems

Microsoft Windows for the host computer and On Time RTOS-32 for the target computer are adopted. RTOS-32 is developed by On Time especially for real-time systems, which makes it possible for the author's platform to have a real-time controlled system. The file size of RTOS-32 is small enough to store all the components on a 1.44 MB floppy disk. This feature is also very important when it comes to an embedded computer system on a robot. For instance, owing to the size, an option to use a light flash card is available. When building power-autonomous robots, it is better to have as little extra weight and space for storage as possible, and a hard disk drive is not desirable.

5-2-2-3. Interface card

An interface card is set up in order to output command signals to the robot and its peripherals as well as to acquire measurement signals from them. The card used in this research is a PCI-3523A from Interface Corporation. It is installed in the target computer and wired to the robot peripheral board built by the author. The board has four D/A terminals for voltage output and eight A/D terminals for voltage data acquisition.

The minimum and maximum voltage of its range are minus10 V and 10 V, respectively. Both D/A and A/D have 12 bits precision.



Figure 20. PCI-3523A from Interface Corporation

The A/D sampling is accomplished through multiplexing and each terminal takes $60\mu s$ to take a sample. As a result, a step of the whole real-time system consisting of the target computer and the robot cannot be any faster than $0.48 ms$ because there are 8 A/D channels. This explains why the control code takes half a millisecond to run. The code itself is small in terms of file size since the applied control scheme is simple, so it does not need much time to execute.

5-2-2-4. Actuator

A SLIP-type robot can be used as a leg module for a multi-legged robot. Basically, if a bipedal running robot is desired, two sets of SLIP modules can be combined, and it is exactly the same design procedure to build a SLIP. In order to take advantage of the SLIP type, one should be aware of power-autonomous robots. The use of a Direct Current (DC) motor would be the best for this purpose.

An R/C servo set – HS-5735MC from Hitec RCD USA, Inc. – is used as a hip actuator. The servo consists of a DC motor from Mabuchi Motor and four stages of

gears with the total gear ratio of 173. The stall torque of the motor is 0.0363 Nm using 8.77 A at 7.2 V . In a compact dimension of $59 \times 29 \times 52 \text{ mm}^3$, the servo includes such a high power motor and high ratio gears. It weighs 146 g .



Figure 21. HS-5735MC from Hitec RCD USA, Inc.

5-2-2-5. Motor amplifier

A 25A8 brush-type PWM servo amplifier from Advanced Motion Controls is used to supply enough power for the DC motor mentioned above so that it will not saturate the commanded current when needed. Available current is 10 A continuously and 20 A for 2 s . The amplifier drives a brush-type DC motor at a high switching frequency. It can be operated in the mode of current control, which enables the author to control the torque of the motor. It is worth using this amplifier because it can measure how much current is output.

The amplifier has a potentiometer to adjust current limit for continuous current. It automatically determines the limit for peak current, which is twice higher than for the continuous current limit value. Although peak current is internally limited by 2 s at maximum, the maximum continuous current in this research is set to be limited at $\pm 5 \text{ A}$ so as to avoid burning out the motor. To make sure, the limitation is also set in the control code that generates and commands the desired current for the motor.



Figure 22. Servo amplifier 25A8 from Advanced Motion Controls

5-2-2-6. Distance sensor

An infrared distance sensor RL50 from STM is selected for a touchdown/lift-off detection sensor. The sample frequency is 500 Hz (i.e. 2 ms per sample). The tip has a diameter of 5 mm and is 13 mm deep. The small size of the sensor enables it to be positioned just beside the toe of the robot in order to detect the ground.



Figure 23. RL50 infrared sensor from STM

The feedback using this sensor causes delays but is not a problem in experiment because the overshoot caused by the delay is empirically adjusted. PD gains are different from simulation because of this. For example, it was observed in experiment that hopping cycles remain stable even if a 20-*ms* delay of lift-off detection occurred. A lift-off detection delay is more likely to happen than a touchdown detection delay because of the double threshold feature of the sensor amplifier, i.e. hysteresis. The threshold is lower when the amplifier goes down to lower voltage to avoid chattering. Moreover, the lift-off angle is a little less steep than the touchdown one. Measuring along the direction of the leg shaft, the distance from the robot's toe to the ground is closer at lift off. For the same body height, touchdown might be detected while lift-off is not.

5-2-2-7. Rotational position sensors

There are in total three angle sensors on the robot and the planarizer. Potentiometers are used to measure the leg angle, and the lateral angle (roll angle) and horizontal angle (yaw angle) of the boom. They are all potentiometers and they do not require counters as needed for encoders. To avoid the complexity of implementation as well as the cost of the parts, potentiometers are a good choice.

A mechanically endless potentiometer N-15 from Piher is attached inside the servo casing in order to measure the leg angle at the hip joint axis. Because it is a through-hole mount type potentiometer, a shaft in the hip axis is put through the sensor. It can rotate mechanically a full 360 *deg* and has the measurement range of 340 *deg*, which is also called electrically effective angle. The size of $16 \times 16 \times 6 \text{ mm}^3$ is also necessary because the sensor has to physically fit in the servo casing.



Figure 24. Endless potentiometer N-15 from Piher

A conductive plastic potentiometer CP-2FK from Midori America Corporation is attached on the joint axis of the base-side boom end of the planarizer. Due to the material of conductive plastic, the potentiometer rotates with little friction. Meaning that the planarizer does not produce unwanted friction. It can also – as the N-15 from Phiher – rotate mechanically 360 *deg* and has the measurement range of 340 *deg* like the N-15 from Piher.



Figure 25. Conductive Plastic potentiometer CP-2FK from Midori America Corporation

A similar conductive plastic potentiometer, WPM 65-20-101 from Waters, is on top of the axis of the planarizer base. It does not cause a lot of friction either and, as is the case with the other models, it can also rotate mechanically 360 *deg* and has the measurement angle of 340 *deg*.

5-2-3. Controller code

5-2-3-1. Overview

The code for controlling the robot is written in Matlab and Simulink packages [57]. The integrator is a 4th-order integrator using Runge-Kutta method. The step time for the integration is of 1 millisecond. This time has been chosen because the code takes half a millisecond to run and twice the amount is reasonable for safety.

The code includes not only a robot control part but also a motor control part and a data acquisition part. The implementation is done as in Figure 25. The controller uses the feedback information from the potentiometer in the hip axis and the STM digital sensor for touchdown sensing. The shaded area is the controller in software. Symbol γ denotes the leg angle and symbol i the current. The appropriate desired angle for a state of the robot is chosen depending on which phase condition the robot is in.

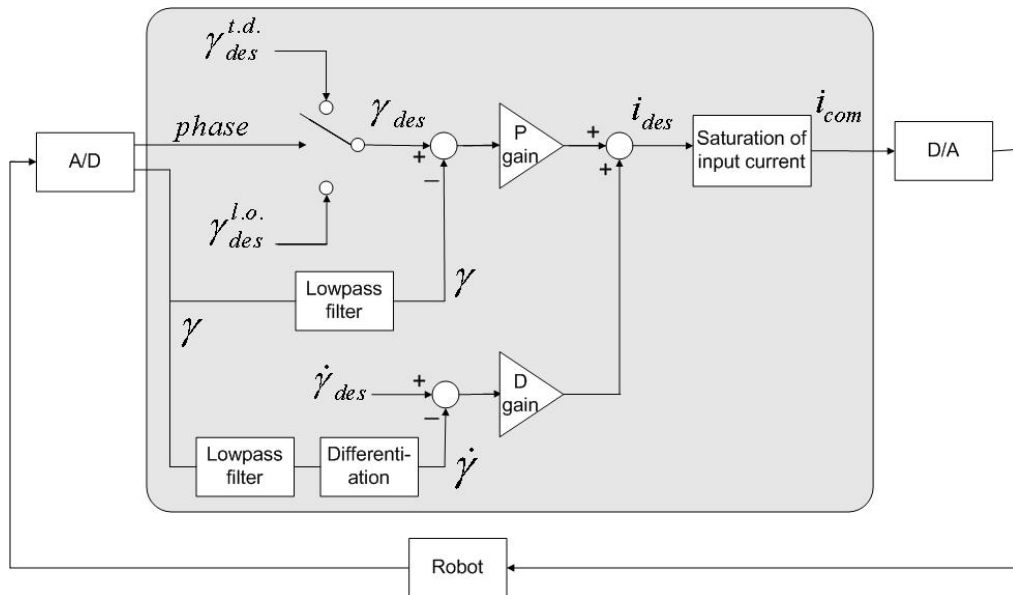


Figure 26. Diagram of the controller in the entire system loop.

5-2-3-2. Lowpass filters

The following 2nd- and 3rd-order lowpass filters are added for the reason that the potentiometer output is noisy:

$$\frac{500}{s+500} \cdot \frac{100}{s+100} \quad (18)$$

$$\frac{250}{s+250} \cdot \left(\frac{60}{s+60} \right)^2 \quad (19)$$

5-2-3-3. PD gains

After the PD gains are set using Ziegler-Nichols Tuning [75], they are adjusted for the follow-through motion of the leg and carefully tuned so that the delay coming from the computer system including the filters will not cause instability.

TABLE V. PD GAINS

Gain term	Phase	Value	Unit
P	Stance	7.248×10^{-2}	<i>A/deg</i>
D		7.248×10^{-3}	<i>A s/deg</i>
P	Flight	8.456×10^{-2}	<i>A/deg</i>
D		5.315×10^{-3}	<i>A s/deg</i>

5-2-3-4. Commanded current limitation

Any exceeding desired current over 5 A is cut down for the safety of the motor and smoother leg motion as set in the simulation. For that reason, the calculated desired current may be greater than 5 A but the commanded current to D/A is never greater than the limitation.

5-3. Methods

The same methods as for the simulation are adopted in order to see the continuity and stability of the robot's hopping behavior.

As described in Simulation implementation, one easy criterion to assess the continuity and cyclic stability of the running motion is to check whether the phase plot for the COM height is a limit cycle and, at the same time, whether the toe clearance is high enough. Phase plots for leg angle and leg length are also designated using the same set of experimental data.

Nine other initial conditions (IC) are also tried in order to see how robust the whole robot of the SLIP mechanism and the controller is. The COM height and the forward speed at apex are used as the state vector of the robot. This is a Poincaré section, and a collection of the initial points at the Poincaré section that converge into a certain cyclic hopping condition in 5 s is obtained as transition plots.

Unfortunately, we do not obtain an experimental region of attraction since the IC's are produced by releasing the robot in the air by hand, and it is difficult to produce 2115 IC's as in simulation results.

Chapter 6: Experimental results

In experiment the robot successfully produces stable hopping that is consistent with the simulation results in Chapter 4. The results are shown by means of plots and images obtained from high frame rate video. The data set used in this chapter is consistently the same set, or some fraction of the same set, obtained from one experiment. The plot for 10 initial conditions (IC's) in Figure 42 is an exception because of 9 other data sets. Discussions are also made along these plots and images.

Note that the actual center of mass (COM) location for the robot body is unlikely at the hip joint. Even from the geometrical point of view, the hip joint is not at the center of geometry of the body shape in the sagittal plane. However, the body cannot rotate in the sagittal plane because it is constrained by the planarizer. Hence, it is correct to regard the hip joint point as the COM location of the robot body. The author calls it the virtual COM of the body, and when it is obvious, it is often just called the COM.

6-1. Motion in the Sagittal Plane

It is likely to be correct that if the robot maintains its condition of a forward speed, an apex height, a hopping cycle, and others at an arbitrary point in hopping cycles,

then hopping motion is stable [16], [79], [42], [44]. In this section, such motion of the robot is checked and discussed.

6-1-1. High frame-rate video

Figure 26 shows sequential snapshots from high frame-rate video. Each interval of the snapshots is approximately 30 *ms* while the frame rate is 250 *frames/s*. Note that the robot moves toward the left in the pictures as time progresses. The first snapshot starts at an apex achieved in the flight phase in a steady-state gait and the last one ends at the following apex. The sequence designates that the dynamical state of the robot at the first apex returns to the same state at the second apex so that the gait can repeat itself indefinitely.

The description on each snapshot is as follows:

1. Flight apex: the leg is vertical. The COM is at the highest point in flight phase. The body is flying down approximately along a ballistic trajectory after this point. The vertical component of kinetic energy is zero. Gravitational potential energy is the maximum.
2. Before touchdown: the leg is being protracted to the desired touchdown angle. The vertical component of kinetic energy is increasing. Gravitational potential energy is decreasing.
3. Touchdown: the leg toe just reaches the ground. The spring is not extended yet but is about to.
4. After touchdown: the leg is being retracted. The spring is being extended (the virtual leg spring is compressed). The body is sliding down along the leg shaft. Kinetic energy is converted to gravitational elastic components of potential energy.
5. Vertical leg: the leg is vertical. The COM is approximately at the lowest point. The vertical component of kinetic energy is zero. The stored potential energy in the spring is about the maximum.

6. Before lift-off: the leg is being retracted to the desired lift-off angle. The spring is being shortened back (the virtual leg spring is decompressed). The body is sliding up along the leg shaft. The restoration of elastic energy provides kinetic energy and gravitational energy. The leg angle determines the distribution ratio.
7. Lift-off: the leg toe is still on the ground but is about to take off. The white leg bushing just hits the upper stopper. The stored elastic energy in the spring during the stance phase is all released.
8. After lift-off: the leg is being retracted for a bit due to follow-through motion and being protracted after that. The body is flying up together with the leg shaft, approximately along a ballistic trajectory. The vertical component of kinetic energy is decreasing. Gravitational potential energy is increasing. The horizontal component of kinetic energy is constant after lift-off.
9. Flight apex: the leg is vertical. The COM is at the highest again. The hopping height is the same as at the previous apex. The vertical component of kinetic energy is zero. Gravitational potential energy is the maximum. This is the initial condition of the next hopping cycle, i.e. the next return map.

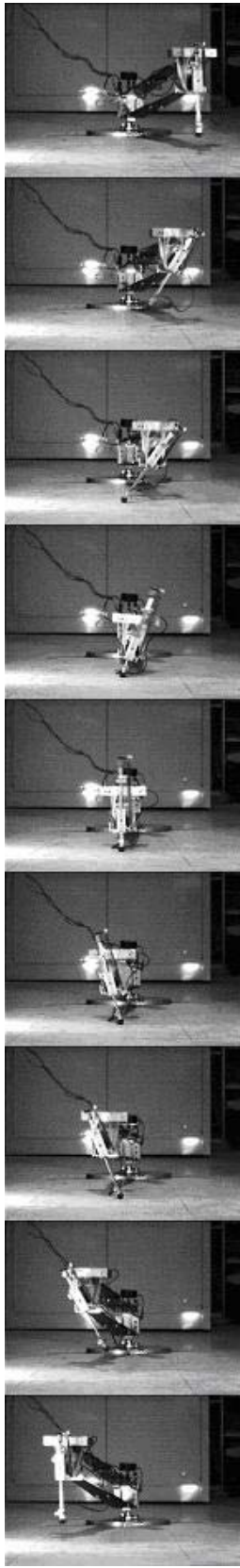


Figure 27. Slow-motion snapshots of hopping motion from an apex to the next apex

6-1-2. Body height vs. horizontal position

Figure 27 shows the locus of the virtual COM of the robot body in the 2D-constraint plane. The data set is from an experiment with an initial forward speed of 0.58 m/s , vertical position of 0.263 m , and vertical speed of 0 m/s .

It shows a non-stop, smooth hopping. The path goes up and down, and at the same time, it always moves forwards except in the first cycle. It does not have any discontinuities, which means that touchdown events are smooth and that the stance dynamics are smooth and are smoothly connected to the flight dynamics.

Even with the initial negative forward speed, it converges into the desired area mentioned in the simulation chapter. Therefore, this implies that small disturbances would not hinder the robot's forward movement. This is demonstrated by the transition plot of 10 IC's later in this chapter.

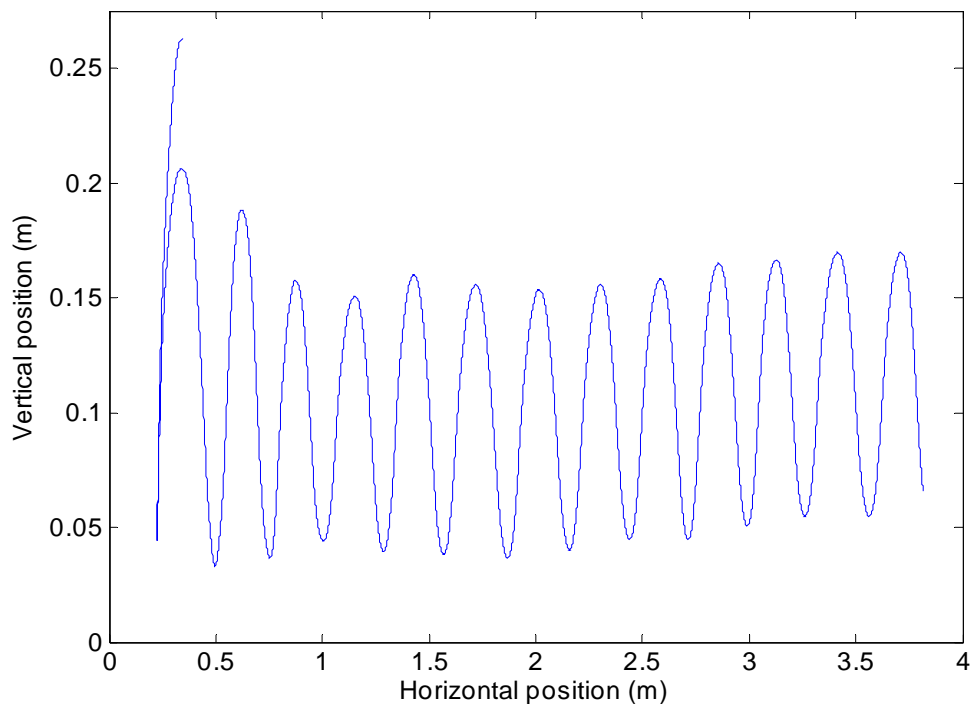


Figure 28. Vertical position vs. horizontal position for the COM with a large error IC

6-1-3. Body height vs. time

Figure 28 is a plot of the height of the COM over time. The hopping height converges into a steady state range. The detected touchdown points are indicated by downward triangles, and the detected lift-off points are by upward triangles. As desired, the touchdown height is lower than the lift-off height so that the proper energy distribution can maintain the robot's condition. The desired touchdown height is $0.12 \cos 40^\circ = 0.092 \text{ m}$, and the desired lift-off height is $0.12 \cos(-25^\circ) = 0.109 \text{ m}$. In the plot, it can be seen that they are not far from the desired values. Because of the delays involved in sensing and filtering discussed previously, the measured values are a little higher than those desired.

In Figure 28, the apex height converges to 0.170 m . This value is as determined in Chapter 2. The bottom height (lowest point in stance phase) is around between 0.050 and 0.060 m . This value range is nearly as desired in the design chapter since the determined bottom height is 0.050 m .

The apex height has 142 % of the rest leg length and the bottom height has 46 % of it. Hence, the height goes up by 42 % and goes down by 54 %, and the total of the vertical distance that the COM travels over a hopping cycle is roughly twice as long the rest leg length r_0 .

The hopping frequency f_{hop} is expected to be 3.0 Hz from the spring stiffness design. Therefore, the expected value for the average speed in vertical motion can be calculated by the total vertical distance traveled divided by the time for one hopping cycle, i.e. twice the leg length multiplied by the oscillation frequency, is:

$$2 \cdot r_0 \cdot f_{hop} = 2 \cdot 0.120 \cdot 3.0 = 0.72 \text{ m/s} . \quad (20)$$

In the actual case, the hopping frequency, f_{hop} , is about 2.8 Hz using the measured average stance duration of 0.16 s and flight duration 0.20 s :

$$f_{hop} = \frac{1}{T_s + T_f} = \frac{1}{0.16 + 0.20} = 2.8 \text{ Hz} \quad (21)$$

Consequently, the actual value for the average vertical speed is 0.67 m/s :

$$2 \cdot r_0 \cdot f_{hop} = 2 \cdot 0.120 \cdot 2.8 = 0.67 \text{ m/s} . \quad (22)$$

This vertical motion might have too big an oscillation amplitude considering that the actual hopping frequency is 2.8 Hz . The robot is subject to significant impact or vibration, and it requires more reliability. In future work, it would be interesting to investigate how to design a hopping robot with less vertical displacement.

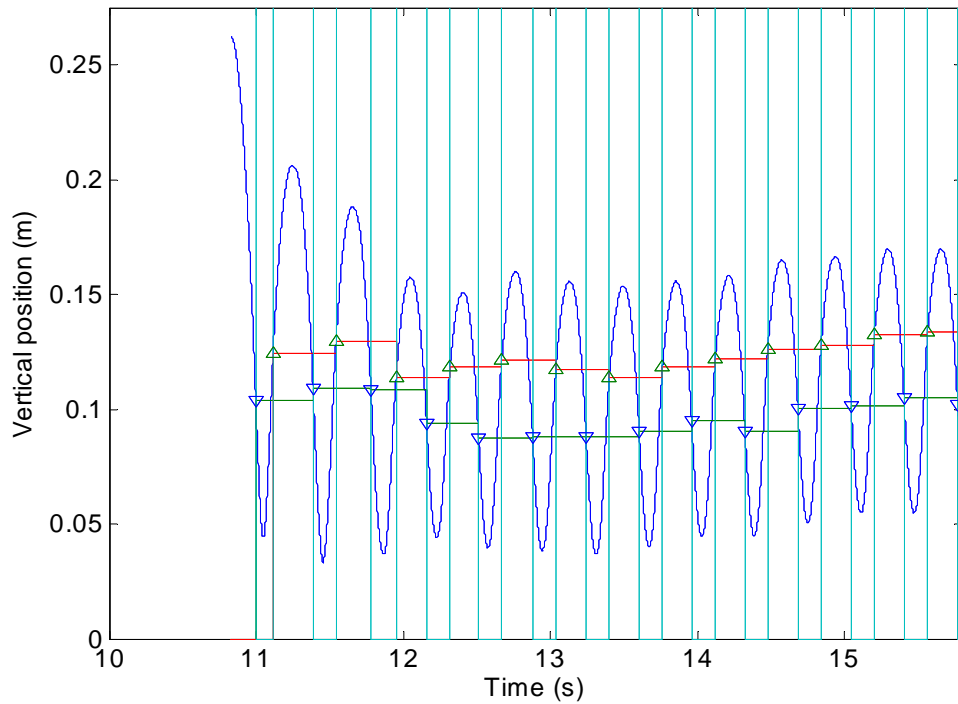


Figure 29. Vertical position of the COM over time

6-1-4. Horizontal position vs. time

Figure 29 shows a plot of horizontal position versus time. It can be seen that the robot moves forwards smoothly and steadily. This plot is monotonous after say 11.2 sec, which means the robot runs almost at a constant speed. The slope can be interpreted as the forward speed. Therefore, it is reasonable to calculate the average forward speed from this plot, and the speed is 0.80 m .

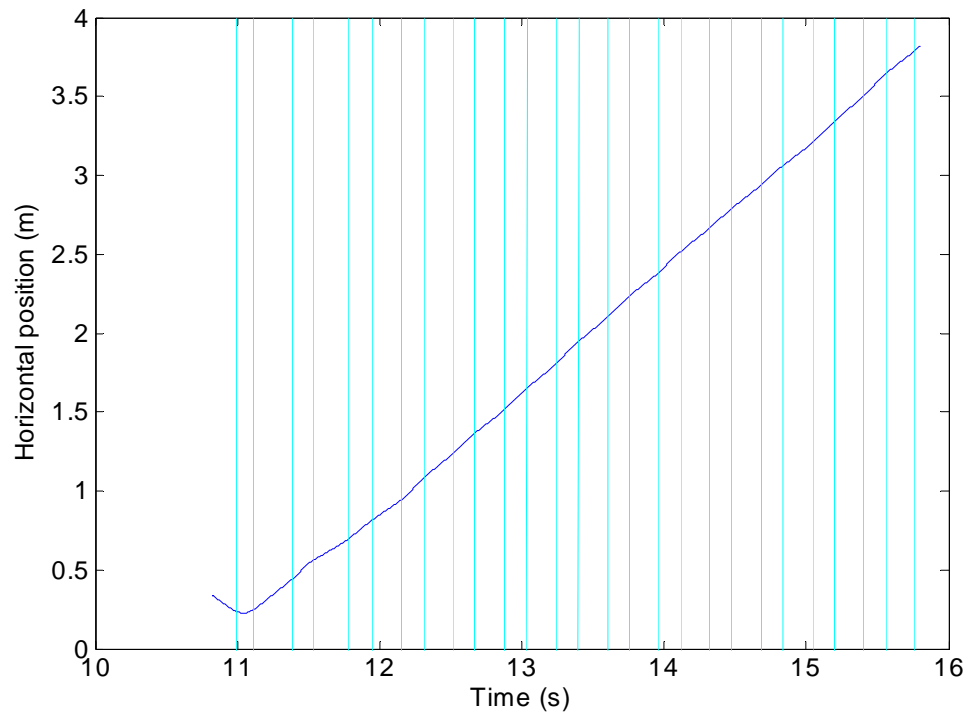


Figure 30. Horizontal position over time

6-1-5. Forward speed vs. time

Figure 30 is a plot for forward speed versus time. The value of the square wave denotes the phase: 0 for stance and 1 for flight. In stance phase, forward speed first increases and then decreases after mid-stance. The slope of the plot is steeper when the forward speed increases. It is because the gravitational acceleration helps when the body goes down along the leg shaft and because the stance-phase PD controller gives

more torque when the leg angle is far from the final set point, i.e. desired lift-off angle, as indicated in Figure 35. When the leg angle comes close to the lift-off angle, the PD controller prevents the body from being quickly rotated about the leg toe. It makes the leg swept slower than just after the touchdown. As a result, the decompressing motion of the virtual leg spring moves the body more likely upwards after the mid-point of stance phase (or mid-stance) and therefore the forward speed decreases.

The forward speed is maximum around mid-stance because of the conservation of momentum. The hip torque is exerted the most in the forward direction when the leg angle is vertical.

In flight, the forward speed curve is almost flat because there is almost no energy input from mechanical work and the body is expected to have a ballistic trajectory in the sagittal plane. Note that the curve is not as flat as expected since the data is created by differentiating horizontal displacement.

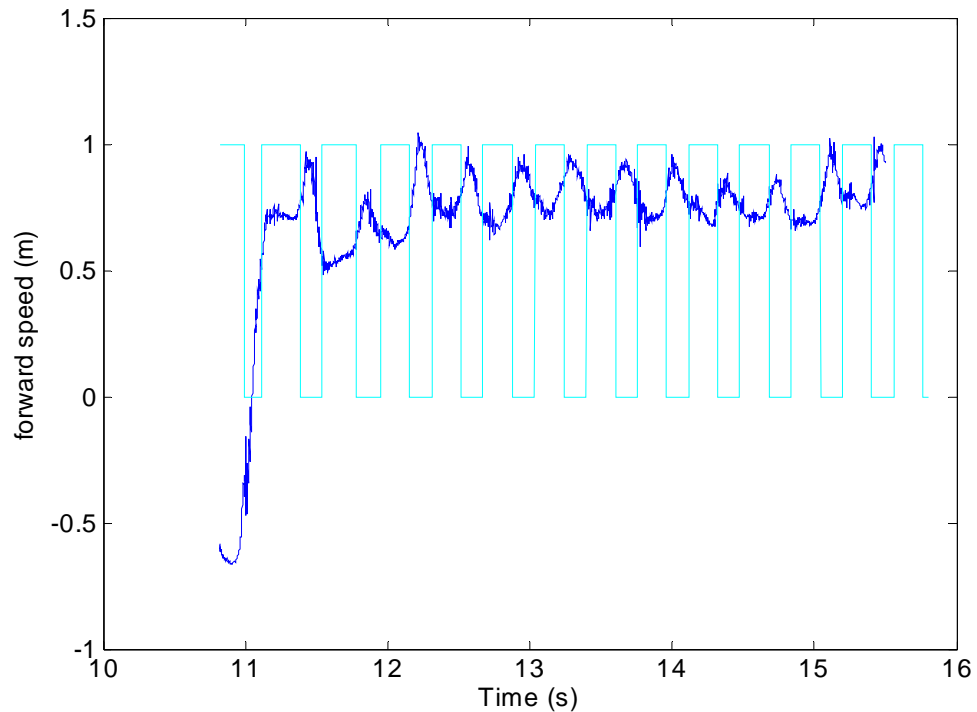


Figure 31. Forward speed over time

6-1-6. Leg length vs. time

For the leg in stance phase, the leg length r is calculated using the leg angle γ and the body height z :

$$r = \frac{z}{\cos \gamma} \quad (23)$$

In flight phase, the leg length is assumed to be constant at 0.120 m , neglecting small vibrations, such as chattering caused by lift-off impact with the stopper. Therefore, as soon as the phase shifts into flight phase, the leg length is set at 0.120 m .

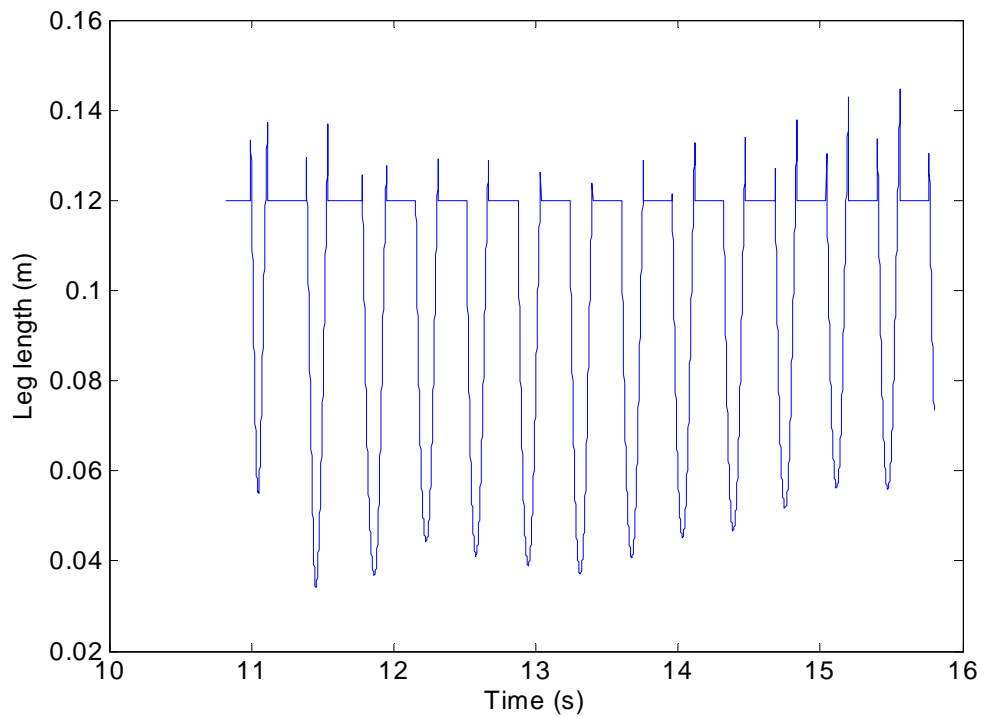


Figure 32. Leg length with error over time

Figure 31 shows the plot for leg length with error over time. Figure 31 has an issue to be discussed. The physical leg length between the toe tip and the hip joint is never longer than 0.120 m , but there are spikes that go way over that value. The spikes happen because of the lead of touchdown detection and the delay of lift-off detection. For the duration in which the body is in flight and in which the sensor still keeps detecting the ground, the calculated value would not be the actual leg length but the distance between the COM and its projected point onto the ground along the leg direction. This appears in the plot as spikes.

The width of the spikes indicates the phase detection time error. As mentioned in the electrical component section, the sample rate of the sensor amplifier is 2 milliseconds. The delay is not only due to the sample rate if the delay is longer than that. In fact, the one at lift-off is longer. When detected, the vertical height of the toe tip at touchdown would be lower than that at lift-off because of the hysteresis and the difference of the two desired angles.

Delay from sensors and filtering exist in every cycle, but the robot continues hopping. Surprisingly, the hopping cycle is still stable. Therefore, the mechanical design and controller design are still valid.

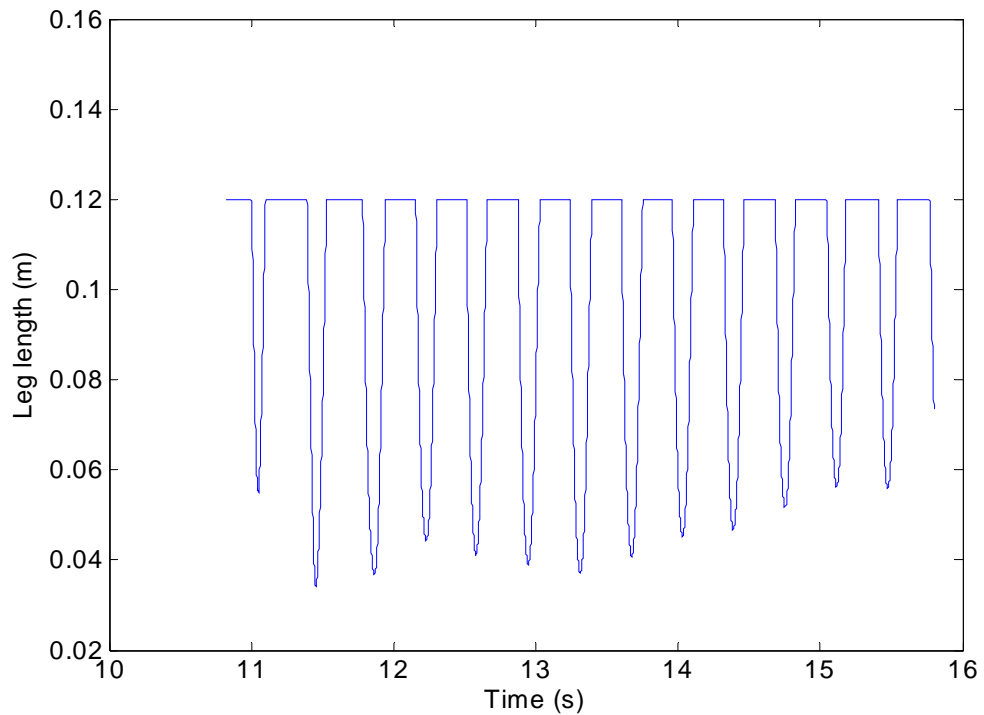


Figure 33. Leg length over time

Figure 32 is the plot with the spikes removed by just cutting them off so as to focus on the behavior of the leg length. The rough shape looks similar to that in vertical hopping as in [16]. This supports the hypothesis that vertical hopping can approximate vertical motion of planar hopping as assumed in the design chapter.

This result also shows that the designed leg length is long enough for this running gait because the COM is always higher than 0.025 m , which is the physical dimension of the robot body from the COM to the lowest part as mentioned in section 2-2-3. *Leg length.*

6-1-7. Summary in hopping motion

It is observed that the robot continuously runs. The followings are also validated:

- Apex height is approximately 0.170 m as desired
- Average forward speed is 0.80 m/s
- There are phase detection errors, but it is acceptable
- Designed leg length is sufficiently long.

6-2. Servo performance

It is essential that the actuator behave as desired. Either controller design flaws or motor performance shortage can cause locomotion failure [27], [19]. In the author's research, both of them must be sufficient in order to protract the leg to the desired touchdown angle and to inject energy for dissipation so that the SLIP can stabilize itself. In this section, the leg control and the motor performance are empirically validated.

6-2-1. Commanded and actual leg angles

Figure 33 is a plot of actual leg angle with the commanded leg angles. The commanded leg angles are 40 deg for stance phase and -25 deg for flight phase. Those angles are the desired angles of the ends of the two phases although those angles are commanded through the whole phases. The leg angle path smoothly alternates between the two phases though the commanded angles are two step inputs. The motion is smooth due to the PD control with low P gains. The plot shows a smooth shape of oscillations in the leg angle. Roughly speaking, this shape is similar to the passive dynamics

trajectory using a hip spring [25], [76], [26]. This supports the justification of the use of PD control in both stance and flight phases.

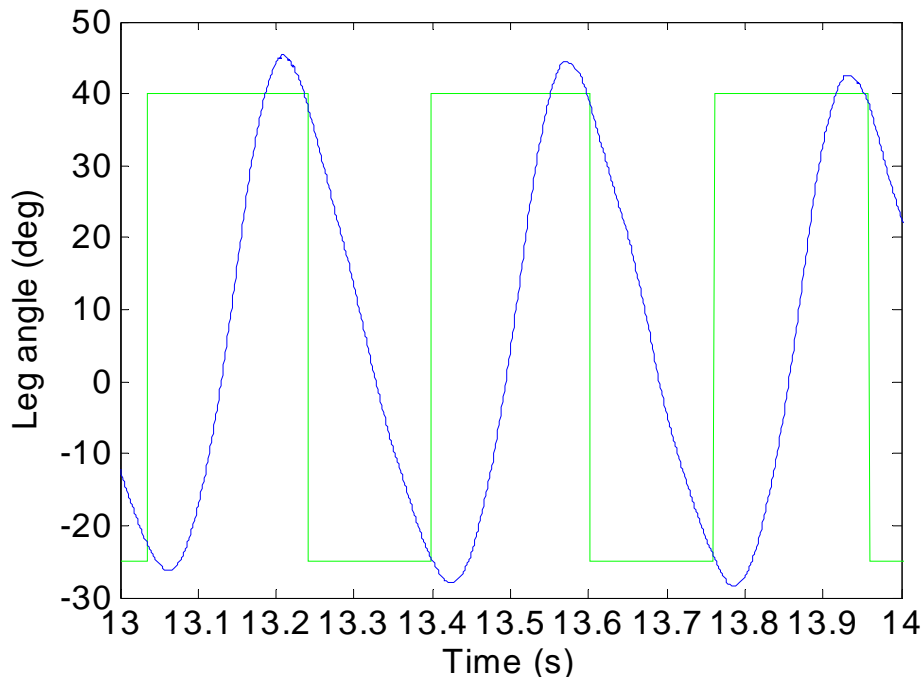


Figure 34. Commanded and actual leg angles vs. time

If a commanded path is impractical to the specifications of the servo system used and beyond the capability of it, it is difficult or impossible to achieve. However, that is not a problem because the commanded square wave is not the same shape as a desired trajectory. The desired trajectory is a trajectory that goes through the desired angles 40 and -20 *deg* at the end of each phase and that goes almost linearly from 40 *deg* to -20 *deg* in stance phase interval and then goes like a 3rd-order spline back to -20 *deg* in flight phase interval. The actual angle trajectory is obtained by tuning PD gains so that it will happen. It results well because Figure 33 shows that the actual path is smooth and meets the requirements.

The imitated 3rd-order-like trajectory should be achieved not by 3rd-order polynomial functions by the square wave and should be satisfyingly accepted. For example, 3rd-order polynomial functions work with practical applications and are often

used for manufacturing robotic manipulators in industry so that their trajectories have smooth paths. If its implementation were needed on the robot in this research, its controller would need a position measurement and a reliable speed measurement. It would heavily depend on the accuracy of sensors. A small delay of measurement might fail to produce a trajectory without discontinuity. Since the robot cannot have a smooth speed measurement in real-time owing to the noisy potentiometer output and physical limitation of the robot size, the real-time generation of a desired 3rd-order trajectory is not an option. Moreover, the use of 3rd-order trajectories requires a high tracking performance, i.e. high gains. However a high gain cannot be used for a derivative gain because of the noisy measurement and differentiation result. It will easily cause instability. These are why the desired leg angle trajectory should be achieved without 3rd-order polynomial functions. The question has been whether or not it can be realized, and it is demonstrated.

In summary, it is demonstrated that the controller is practically good enough and reduces calculation cost and hardware cost by exploiting the tracking characteristics of PC control with low P gains.

6-2-2. Desired, commanded, and actual current

Current control, not voltage control, is used for the DC motor by using the motor amplifier described in *Chapter 5: Experimental setup*. Current, which is proportional to torque, is the desired output from PD control. The PD gains were tuned in such a way that the maximum desired current would be about 7 A while the maximum current that the amplifier can provide is 5 A. This results in a saturation of the control at large errors.

In Figure 34, as a result of this limitation, the desired current is saturated and the commanded current is constant in the beginning part of each phase. For the rest part, the actual current tracks the commanded current trajectory well.

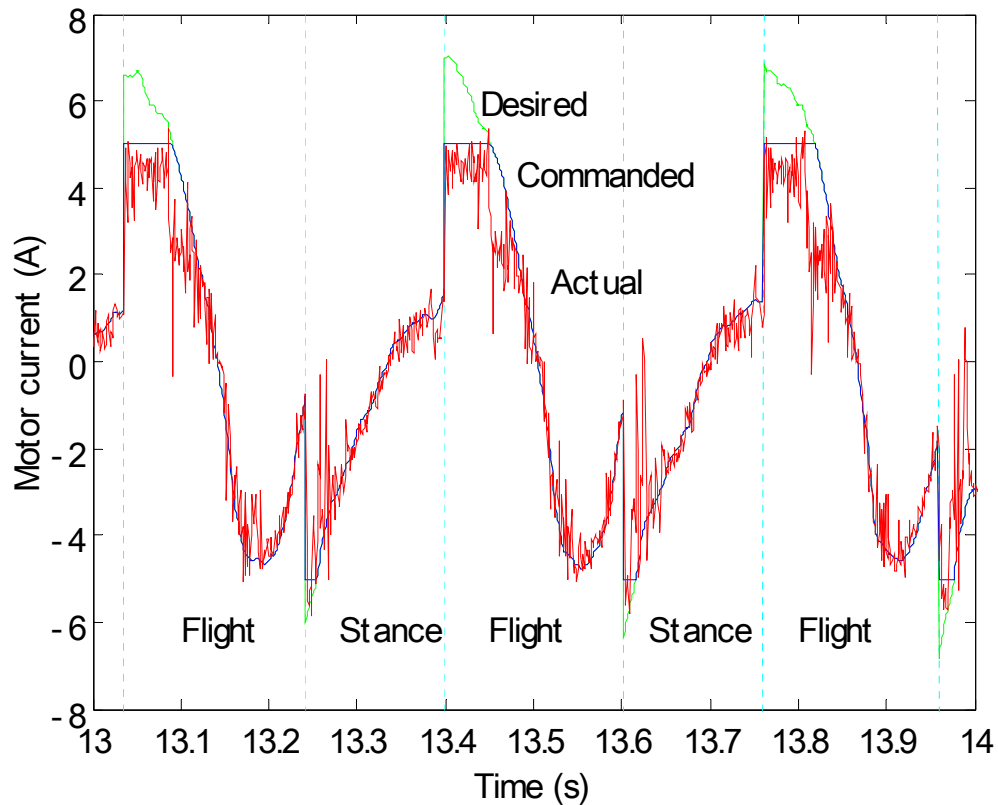


Figure 35. Desired, commanded, and actual current vs. time: positive current protracts the leg in flight and negative one retracts it in stance

The required power in flight is higher than in stance. That matches with the result of the hip motor energy cost of Monopod I in Gregorio's *et al* research [77]. The dynamics of a Spring Loaded Inverted Pendulum (SLIP) without any actuator by nature has the leg sweeping in stance if the SLIP brings the leg to a proper angle at touchdown and if friction and impact are not severe. Therefore, it takes more power to swing the leg forwards in flight phase so as to place it to the desired angle.

6-2-3. Torque-speed curve

It is fundamental to compare the actual torque-speed curve to the maximum performance hexagon. It should not command any higher current than the motor can handle. Not only may it cause too much heating but also the controller will not work as

wished due to saturation. For example, model-based control would not work for the applications with low-performance servo systems [27], [19].

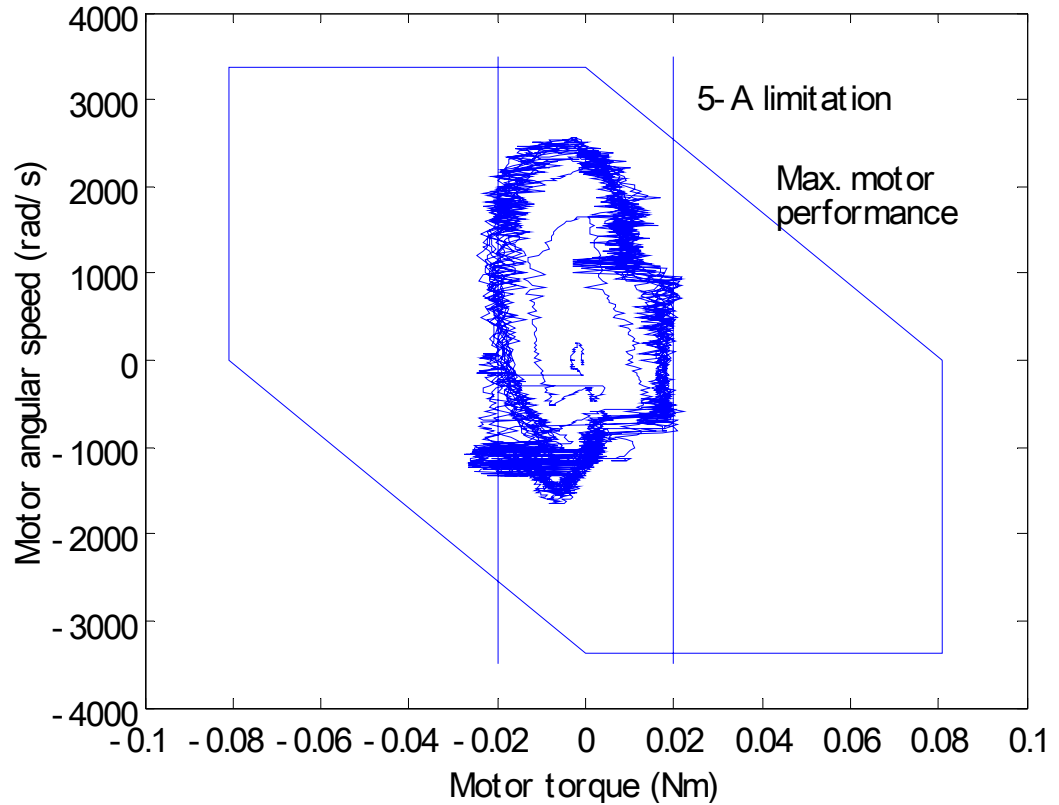


Figure 36. Torque-speed curve of the motor

The hexagon in Figure 35 is the maximum performance curve of the motor alone without gears. The two vertical lines show the maximum possible torque with the 5-A limitation. The plotted signal is for the actual torque-speed curve of the motor. The curve corresponds to 14 hopping cycles.

The actual motor torque is approximately estimated using the formula:

$$\tau_{motor,estimated} = K_{\tau} \cdot i_{actual} \quad (24)$$

where $\tau_{motor,estimated}$ is the estimated torque in the motor output axis, K_t is the torque constant of the motor, and i_{actual} is the measured current in the motor amplifier.

The motor speed is obtained by multiplying the hip speed by the total gear ratio of the 4-stage gears from the motor axis to the hip axis:

$$\omega_{estimated} = \dot{\gamma} \cdot R_{gear} \quad (25)$$

where $\omega_{estimated}$ is the motor speed, $\dot{\gamma}$ is the angular speed of the leg at the hip, and R_{gear} is the total gear ratio. In spite of the fact that there is some uncertainty on the calculation and measurement, especially at a transient state for backlash, it should be correct at a relatively steady speed.

In Figure 35, it can be seen that the actual motor curve absolutely stays inside the maximum motor curve hexagon and mostly fits in the domain created by the hexagon and the vertical lines. Thus, the motor specifications are sufficient and the current limit might not be high enough. The sufficiency of the current limit value is discussed next.

The actual curve goes a little outside at the bottom left part. It can be explained using Figure 34. The actual current in flight phase does not much exceed the line at 5 A. On contrary, the one in stance phase goes lower than the line at -5 A more often. It happens just after touchdown because of touchdown impact with sudden load torque from ground force. Consequently, more current is drawn. Nonetheless, the impact is not so big that it can disturb the control of the motor and the smoothness of the leg angle trajectory in Figure 33. Hence, the absolute value of the current limit is high enough at 5 A.

6-2-4. Summary of motor control performance

- Leg motion is well controlled as desired
- Actual motor current tracks commanded trajectory well

- Servo system specifications are sufficient and the current limit is high enough.

6-3. Stability

Figures in this section show phase plots, transition plots of apex height. Such plots can be used to examine a 2-D cross-section of the state space of a dynamical system and show convergence itself.

6-3-1. Phase plot of vertical height

Figure 36 is the phase plot of the height of the COM (i.e. plot of vertical speed vs. vertical position). This is from the same set of experimental data considered earlier. The left part represents stance phase, and it is a harmonic system. In flight, it is a ballistic trajectory. From the stance phase in the 1st cycle, the trajectory goes towards inside. The combination of the two dynamical characteristics creates a closed orbit and remains tracing on the same course over cycles. A stable limit cycle is obtained.

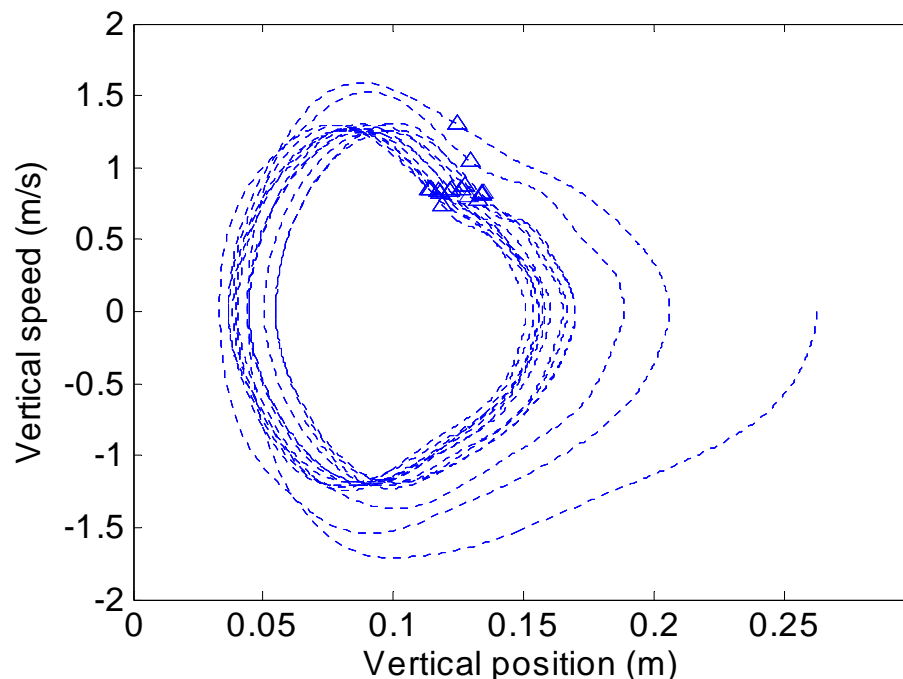


Figure 37. Phase plot for the vertical position of the COM

6-3-1-1. Stance phase and energy balance

The path in stance phase is a smooth curve. This suggests that the hip torque injects sufficient mechanical energy into the robot by sweeping the leg. The amount of input energy is just the amount the robot would lose by dry friction, viscous damping, and impact if there were no hip torque. Otherwise, hopping cycle would collapse and the path would get away of the closed orbit either inwards or outwards.

The plot shows the energy conversion between kinetic energy of vertical speed and gravitational potential energy of height. However, the plot does not have the axis for forward speed nor that for spring deflection, so the plot does not designate the energy conversion between that of forward speed, that of vertical speed, and that in the spring. For instance, if forward speed at touchdown is turned into vertical speed at lift-off as in Figure 7(b), the orbit does not explicitly show it and the radius increases. For elastic potential energy during the stance phase, it is being stored after touchdown at the bottom edge of the orbit, and then, it is being released after the left edge until the top edge. It can be seen that the vertical position does not change much but the vertical speed increases.

6-3-1-2. Flight phase and leg model error

In flight phase, the path should ideally follow a smooth curve. After lift-off, however, there is a slight bump. Both position and speed increase sharply at the triangle marks a while after the leg takes off. Since it does not happen soon after lift-off, it is not because of the impact on which the upper leg bushing hits the end of travel as Koechling indicated [64]. It is probably because of the leg swinging as McMordie proposed [65]. The following two forces act between the robot's body and its leg:

- Centripetal force $F_{cent} = m_{leg} \dot{\gamma} / r$ as the leg is rotating
- Vertical element of reaction force for acceleration $F_{iner} = \tau r \sin \gamma$.

Before lift-off, the leg is swept backwards and the direction of the electrical current into the motor (i.e. the direction of the hip torque) is negative. When lift-off is detected, the hip torque changes to positive. When the leg starts to be protracted, the vertical speed of the leg's COM goes down and as a counter-action, the speed of the body's COM goes up. After the leg passes the vertical line, that of the leg's COM in turn goes up and that of the body's COM goes down. As a result, the trajectory of the body's COM for the flight phase is not a perfect ballistic trajectory while an idealistic point-mass system would produce it.

Owing to the assumption of a mass-less leg, this bump does not appear in the phase plot in simulation. In simulation, phases are discontinuously connected at touchdown/lift-off events and there is no bump after lift-off.

6-3-1-3. Symmetry

Last of all, the outline of the orbit is symmetric with respect to the line for zero vertical speed as the ideal SLIP model has been shown to be [16], [45]. It shows that the motion from an apex to the following apex is symmetric. The compensation of the energy loss is well handled by leg sweeping in stance.

6-3-2. Phase plot of leg angle

Figure 37 is the phase plot of leg angle γ (i.e. plot of leg angular speed versus leg angle). Time progresses clockwise. Touchdown occurs at the right bottom corner. Lift-off does at the left bottom corner. The measured states at touchdown and lift-off are shown as downward triangle marks (∇) and upward triangle marks (Δ).

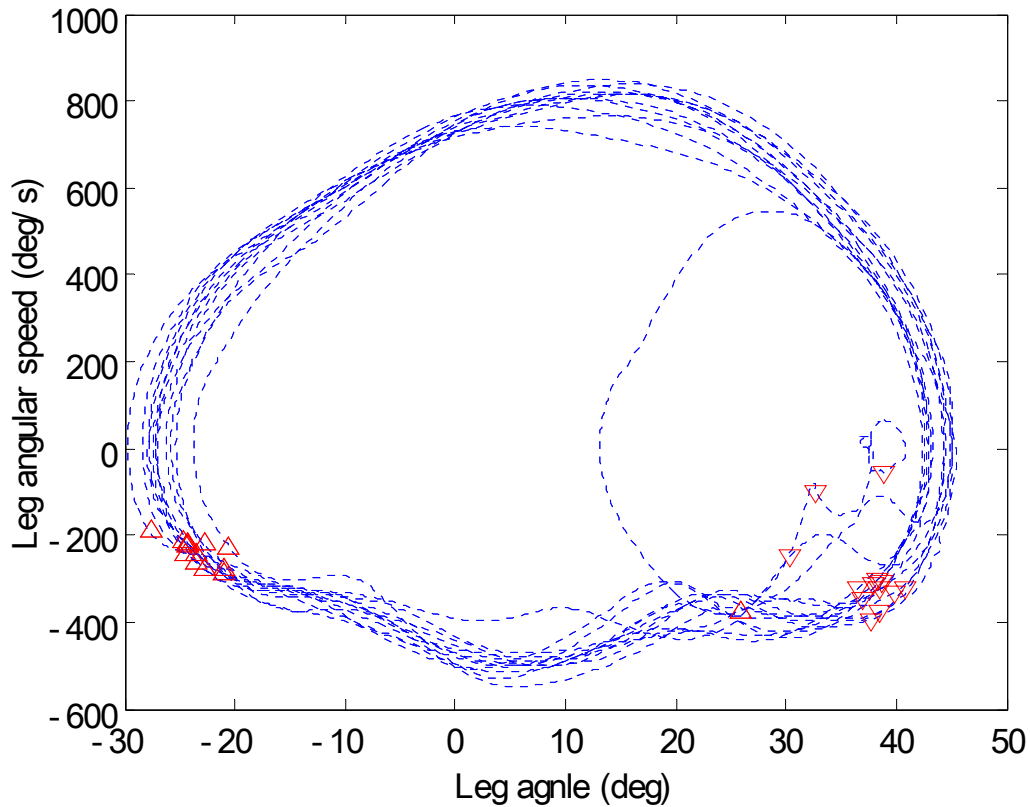


Figure 38. Phase plot for leg angle

6-3-2-1. Commanded and actual angles and limit cycle

The commanded states of leg angle and speed are 40 deg and 0 deg/s for touchdown and -25 deg and 0 deg/s for lift-off. By inspecting the downward triangle marks, however, it can be seen that the states at touchdown for the first three cycles are out of the main orbit, that the curve converges to the limit cycle so that the rest of the states at touchdown goes on the orbit, and that those commanded states are not achieved since the leg speeds are not 0 deg/s . In fact, the author avoids them intentionally and exploits two characteristics of the SLIP model dynamics and PD controllers: the follow-through motion at the beginning of flight and the overshoot at the end of flight as described in section 6-2-1. *Commanded and actual leg angles*. Owing to this, the path becomes a closed orbit without discontinuity.

6-3-2-2. Symmetry

The orbit of leg angular speed versus leg angle is roughly symmetric with respect to leg angle. The symmetry line for the lower stance-phase part is approximately at 8 *deg* compared to the symmetry line for the ideal SLIP model is 0 *deg*. In spite of the fact that the hip torque does not increase in the middle of stance in Figure 34, the angular speed is the fastest in Figure 37. That indicates that the minimum leg length probably happens right there. This angle is the shifted amount of the mean angle of the leg sweeping (7.5 *deg*) as mentioned in the section for touchdown/lift-off angle design. Thus, the angle shifting is successful without destroying the symmetry of the SLIP model property [47], [48], [49], [45].

The orbit is not perfectly symmetric. In stance, the leg actuation requires more torque for the first half due to the gravity on the body than for the second half. In flight, the leg swinging needs more torque for the second half due to the gravity on the leg. The angular speed in flight is fast in the first half, and the symmetry line for the upper flight part is at approximately 12 *deg*.

6-3-3. Phase plot of leg length

Figure 38 is the phase plot of leg length r (i.e. plot of leg length versus derivative of the leg length). Except the line on the right edge, the data of the plot correspond to stance phase. The line on the right edge corresponds to flight phase. The left rounded edge indicates the bottom in stance. At this point, the leg length is the minimum, and the derivative of that is zero. The time progresses clockwise along the orbit

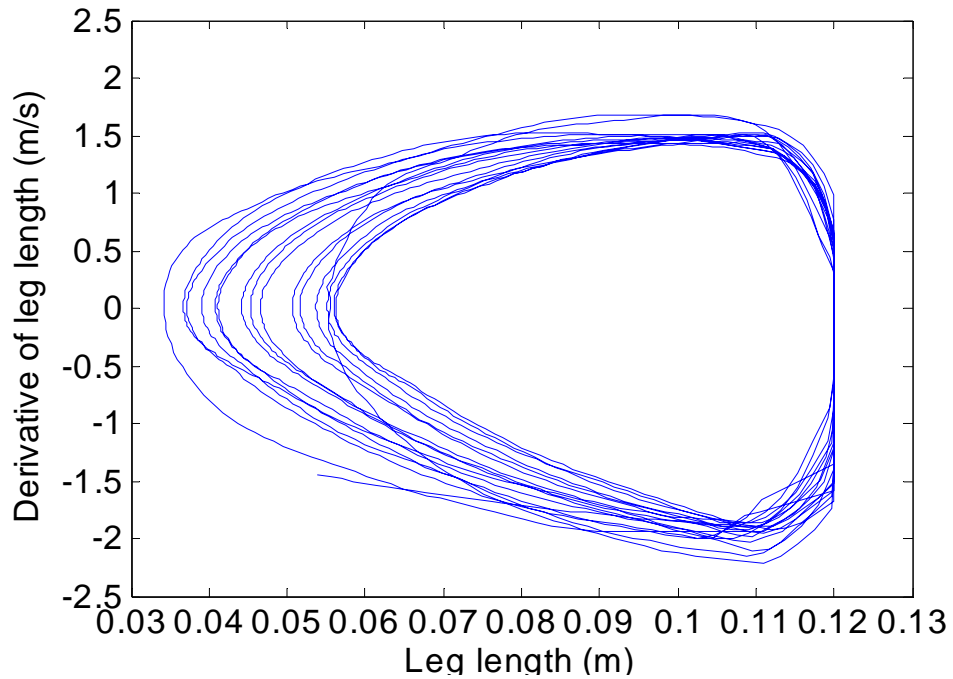


Figure 39. Phase plot for leg length

6-3-3-1. Error

On this right straight line, the leg length is 0.120 m and does not change throughout flight phase, so the derivative is supposed to be zero all the time. Consequently, the plot for flight phase is supposed to stay at point $(0.120, 0)$. In other words, except this point, the path is supposed to be for stance phase. Therefore, it is ideally expected to stop and stay at that point while in flight. However, it is not a point but a line in the obtained data because of the ground sensing error.

Even when the leg toe is off the ground, the sensor still continues detecting it about 10 ms after lift-off (in order to ensure the high height after lift-off and the enough toe clearance in leg protraction in flight) and before touchdown (in order to cancel out rise time and prepare for leg retraction). This lead/delay of the ground detection incurs error in the phase plot because it causes leg length value to be longer for the distance between the toe tip and the ground than the physical limit of 0.120 m .

This error is a problem because leg length is not directly measured. For stance phase, leg length is obtained by applying a trigonometric function to the measurements of COM height and leg angle. For flight phase, leg length is set 0.120 m . Therefore, if

phase change is not accurately sensed, it invites error in leg length calculation, i.e. the right edge part becomes to be composed of not points but lines.

The error part of the leg length longer than 0.120 m is different from the actual motion of the robot. Therefore, leg length data that have bigger values than the rest leg length are cut off. As a result, it seems as if the derivative of leg length were changing while leg length were constant at 0.120 m . Not only the ideal flight phase point ($0.120, 0$) but also the straight line is the data for flight phase. The maximum error in the derivative is approximately -1.7 m/s at lift-off (the bottom-right corner of the phase plot) and 1.0 m/s at touchdown (the top-right corner). The error is bigger at lift-off owing to the difference of the desired touchdown/lift-off angles and the hysteresis of the ground detection.

6-3-3-2. Symmetry

Though the outline of the orbit is roughly symmetric, it is not precisely symmetry. The lower part is more dilated because the sweeping angle from touchdown to the vertical line is wider than the rest.

Biological research work has been done on planar hopping dynamics and vertical hopping dynamics [31], but, to the author's best knowledge, no rigorous analytical result is known about leg length dynamics in planar hopping [16]. However, the expansion of the lower orbit can be explained as follows.

In the case of this research, a PD controller is used for stance phase. The controller retracts the leg fast after touchdown because the touchdown angle is far from the final set point. Therefore, the leg length is shortened fast until leg angle reaches the vertical line. Consequently, the leg spring gets compressed faster than it would in vertical hopping because the leg retraction itself helps reduce the leg length. In addition to that, the gravity also helps. The curve for the first half of stance dilates more outwards.

After the leg passes the vertical line, on the contrary, the leg length more slowly goes back to the rest length because the desired angle is closer and the gravity works in the opposite direction of spring decompression.

6-3-4. Vertical position phase portrait time evolution

Figure 39 shows a plot of vertical speed versus vertical position over time. The circular shape is created by the 2D cross-section of the vertical position and vertical speed states, and one turn of the spiral designates one hopping cycle as in the case of the 2D plot without time axis. The time transition of the cross-section appears as the progress in the direction of spiral axis, and therefore, the pitch length of the spiral indicates the period of one hopping cycle.

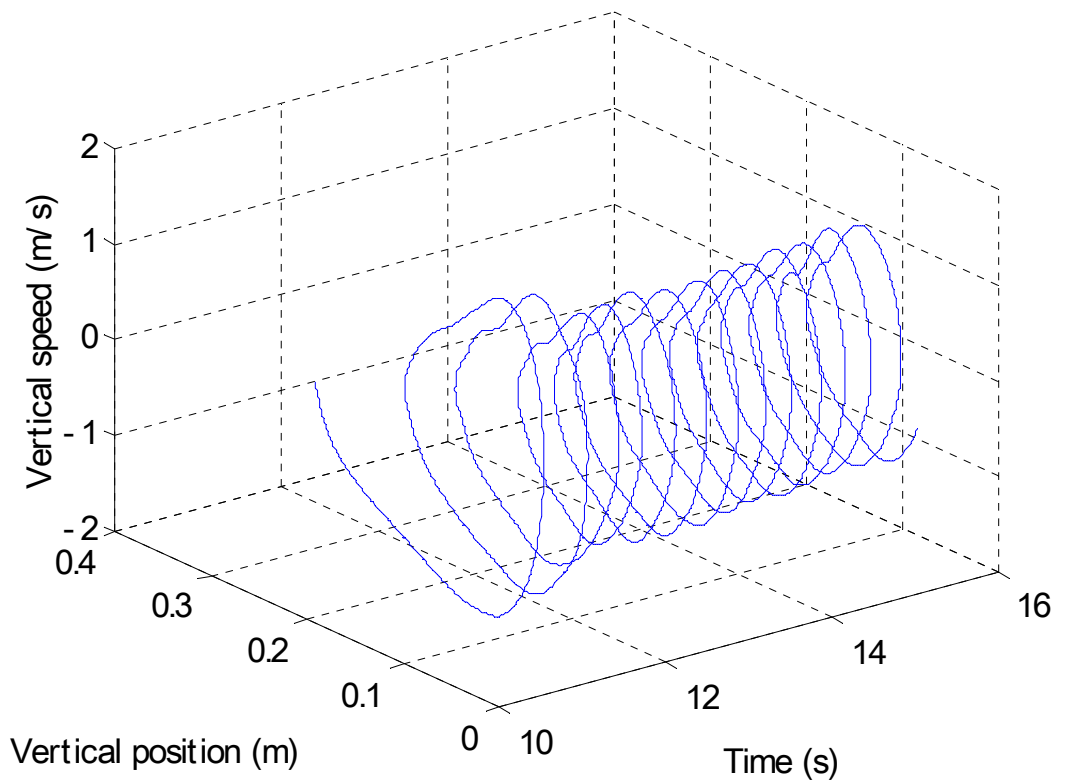


Figure 40. Vertical position phase portrait time evolution

It can be seen that the initial conditions leads to a cyclic spiral. In this experiment, the initial point is set to be at apex, so the speed is always 0 *m/s* at the starting point. The initial point only depends on the height.

While the 2D phase plot shows variation by the thickness of the orbit, the 3D phase plot shows the path of each hopping. If one path goes away from the average path, it will appear as a bump of the spiral pipe.

6-3-5. Transition plot

Figure 40 shows a transition plot of forward speed and vertical position, i.e. a sequence of the state vectors at apex, for the experimental data set. (“Transition plot” is the author’s term. For more details on the transition plot, please see section 3-2-2-6. *Transition plots and regions of attraction.*) The state vectors transit via the return map from an apex to another. Some researchers in legged locomotion use apex for a return map section [62], [45], [15] because vertical speed axis is not needed since it is 0 m/s at apex and therefore, only the two variables are needed to check a hopping condition. The vertical speed is 0 m/s and the elastic potential energy is constant for any apex condition. Hence, forward speed and height at apex represent the mechanical energy of the robot.

The IC point of apex leads to convergence to the neighborhood of the desired point even though the IC is distant from the desired values of forward speed 0.80 m/s and vertical position 0.170 m . Note that the plotted value is at apex and its forward speed should be lower than the target average speed 0.80 m/s as explained in *Chapter 4: Simulation results*. The IC in this experiment converges in a similar way to the IC in the simulation. This IC in experiment is forward speed -0.58 m/s , vertical position 0.263 m , and vertical speed 0 m/s while the IC in simulation is forward speed -0.60 m/s , vertical position 0.260 m , and vertical speed 0 m/s . Considering the difference, it seems that the plotted result matches with the simulation result.

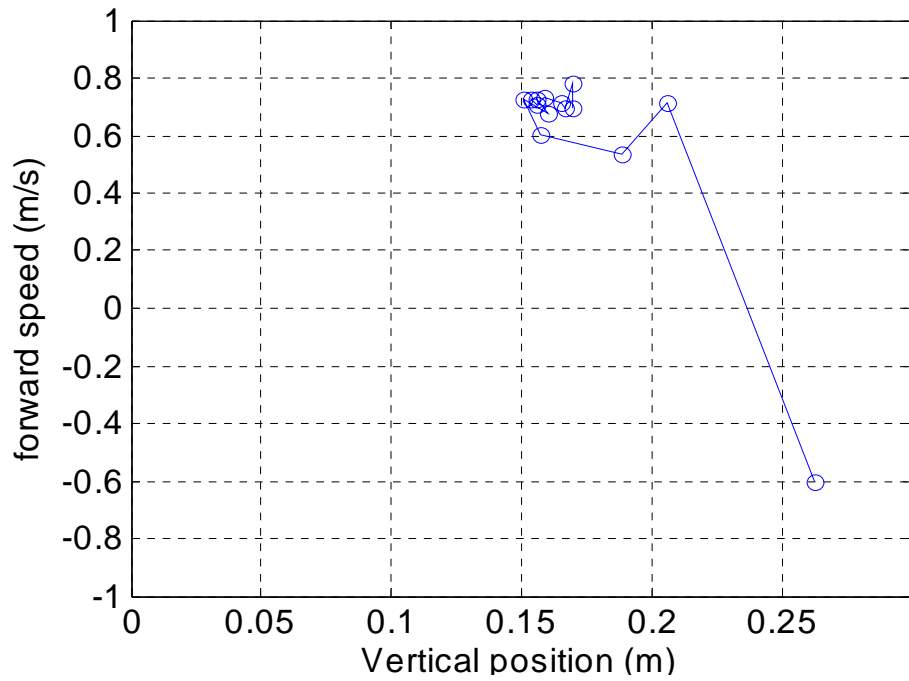


Figure 41. Transition plot for an IC with large error

6-3-6. Experimental region of attraction

As explained in section 5-3. *Methods*, the plot for 10 transitions is obtained as in Figure 41. (The data set used up to now and 9 additional data sets.) Accordingly, no boundary of the domain of all the converging IC's can be presented. In other words, the region of attraction for the SLIP robot on experiment cannot be determined.

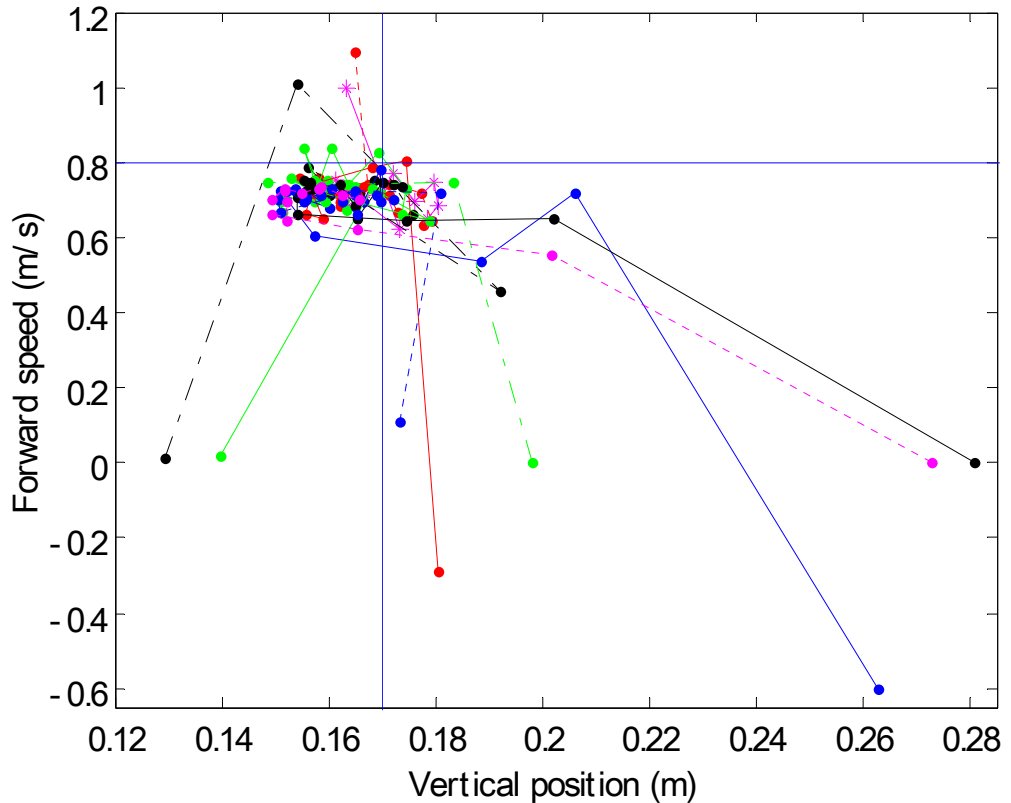


Figure 42. Converged transitions for 10 IC's

All the 10 IC's go to the approximately same desired area, as in the simulation, and it indicates a large region of attraction as in the simulation result of Figure 13. It demonstrates that a few of IC points near the edge of the simulation region of attraction also converge. The experiment to some degree has validated that the author's SLIP-based design is viable and that the stability of the gait is robust.

If reasonably small enough disturbances are added to the robot, it will remain in a recoverable state and restore it to a stable condition in several hopping cycles. The acceptable magnitude of disturbance is such that the robot's condition stays within the condition equivalent to the region of attraction after receiving a disturbance. If the state at the following apex is within the region, the robot can certainly converge its state into a stable one as if it started its hopping at that apex. For example, if some object hits the robot during its flight or the leg toe lands on a stair step with a different height, the

condition after the disturbance can be regarded as its initial condition to restart its hopping.

6-3-7. Summaries in stability

- Phase plots show that cyclic motion is achieved in terms of COM height, leg angle, and leg length
- The hopping is robust within a certain range of apex conditions for height and forward speed.

Chapter 7: Conclusions

7-1. Conclusions

This thesis has presented the development of a SLIP-model-based hopping robot. To the author's best knowledge, this thesis is the first publication that ever demonstrated the design, simulation, mechanical implementation, and experimental results of the SLIP model, which has been validated only in the field of biomechanics and dynamical analysis within the last three decades [10], [11], [12], [13], [14], [9], [45].

The essential three parameters (mass, leg spring stiffness, and leg length) of the SLIP model were determined. A simple controller for a SLIP model was created and resulted in stable running in simulation. Next, a miniature one-legged hopping robot with only one actuator at the hip joint was constructed, and stable running was experimentally demonstrated. Both simulation and experimental results indicated a large region of attraction for the desired running behavior. The following goals are achieved:

- Feasibility study of the realization of the SLIP model
- Design and construction of a SLIP robot hopper with one actuator
- Experimental implementation of a simple controller on the SLIP
- Experimental validation of the SLIP model

- Demonstration of a robust hopping robot with only one actuator in the hip.

From these developments, the following conclusions may be drawn:

- The SLIP model with the three parameters (mass, leg spring stiffness, and leg length) has been validated.
- A simple controller for the SLIP-model-based robot has resulted in stable running in simulation and by experiment. The only necessary energy input was to replace losses and the only balancing control that might be necessary would be to correct for the touchdown angle of the leg. This is consistent with the self-stability property of the SLIP model [22], [23], [24].
- Simulations and experiments have indicated a large region of attraction for a robust running behavior. The SLIP model might also be applicable to the running of animals and humans on non-level surfaces.

Though these conclusions are as desired, the tested conditions in running speed, in general, the touchdown leg angle and others are not general. It would be necessary to accomplish the same results for different conditions in order to completely conclude the validity of the SLIP model.

7-2. Future work

The author first suggests such future work as speed control for different desired speeds and height control for different desired heights. For speed control, Raibert's forward speed controller [16] might directly be applied. If so, only the measurement of stance duration would be required to be added to the author's robot. For height control, a novel control method might be required if an additional actuator to the prismatic joint along the leg is not an option.

The implementation of a SLIP robot without the support of a planarizer is the next suggestion. It would be much more complex because a single-leg hopping in 3D requires another actuator and the COM of the body must actually be aligned in the hip joint in order to exploit the results of the author's work. The two matters will require a major refinement of the mechanical structure design.

With a single-leg hopping in 3D, it will be mandatory to add another actuator in the hip and control the body in the lateral plane as well as in the sagittal plane.

The second matter can be avoided by realizing a control method for the SLIP model with pitching dynamics. That SLIP model is not yet the main stream because it is relatively new, but several papers on analysis and simulation have been published [45], [78]. The position and inertia of the COM of the robot body have to be taken into consideration for running controllers so that the hip torque does not spin the body.

Bibliography

- [1] D. Wettergreen, C. Thorpe, and W.L. Whittaker, "Exploring Mount Erebus by Walking Robot," International Conference of Intelligent Autonomous Systems, pp. 72-81, 1993.
- [2] Robin R. Murphy, "Rescue Robots at the World Trade Center," Journal of the Japan Society of Mechanical Engineers, special issue on Disaster Response Robotics, vol. 102, no. 1019, pp. 794-802, 2003.
- [3] Kazuo Tani, Kiichi Ikeda, Tomoaki Yano, Shuuji Kajita, Osamu Matsumoto, "The Concept of Model Free Robotics for Robots to act in Uncertain Environments," Proceedings of the 1993 IEEE/Tsukuba International Workshop on Advanced Robotics, pp. 85-90, Tsukuba, Japan, 1993.
- [4] S. Kajita, and K. Tani, "Adaptive gait control of a biped robot based on realtime sensing of the ground," Proceedings of IEEE International Conference on Robotics and Automation, pp. 570-577, 1996.
- [5] Jessica Hodgins, "Legged Robots on Rough Terrain: Experiments in Adjusting Step Length," Ph.D Thesis, Dept. of Computer Science, Carnegie Mellon University, Pittsburgh, Pennsylvania, 1989.
- [6] S. Kajita and K. Tani, "Study of dynamic biped locomotion on rugged terrain - Derivation and application of the linear inverted pendulum mode -," Proceedings of the IEEE International Conference on Robotics and Automation, pp.1405-1411, 1991.
- [7] P. V. Nagy, W. L. Whittaker, S. Desa, "A Walking Prescription for Statically-Stable Walkers Based on Walker/Terrain Interaction," Proceedings of the IEEE International Conference on Robotics and Automation, pp. 149-156, 1992.
- [8] Pearson Education, Inc., "Speed of Animals," Fact Monster, <http://www.factmonster.com/ipka/A0004737.html> , 2000.

- [9] R. J. Full, and D. E. Koditschek, “Templates and anchors: Neuromechanical hypotheses of legged locomotion on land,” *Journal of Experimental Biology*, vol. 202, pp. 3325-3332, 1999.
- [10] R. McN. Alexander and A. Vernon, “Mechanics of hopping by kangaroos (Macropodidae),” *Journal of Zoology*, London, vol. 177, no. 265-303, 1975.
- [11] R. M. Alexander and A. S. Jayes. “Vertical movement in walking and running,” *Journal of Zoology*, London, vol. 185, pp. 27-40, 1978.
- [12] R. Blickhan, “The spring-mass model for running and hopping,” *Journal of Biomechanics*, vol. 22, pp. 1217-1227, 1989.
- [13] R. Blickhan and R. J. Full. “Similarity in multilegged locomotion: Bouncing like a monopode,” *Journal of Comparative Physiology*, vol. 173, pp. 509-517, 1993.
- [14] C. T. Farley, J. Glasheen, and T. A. McMahon, “Running springs: Speed and animal size,” *Journal of Experimental Biology*, vol. 185, pp. 71-86, 1993.
- [15] Ioannis Poulakakis, “On the Passive Dynamics of Quadrupedal Running,” M.Eng. Thesis, Department of Mechanical Engineering, McGill University, Montreal, Canada, 2002.
- [16] M. H. Raibert, “*Legged Robots That Balance*,” MIT Press, Cambridge, MA, 1986.
- [17] H. B. Brown, G. Z. Zeglin, “The Bow Leg Hopping Robot,” *Proceedings of the IEEE International Conference on Robotics and Automation*, 1998.
- [18] U. Saranli, W. J. Schwind, and D. E. Koditschek, “Toward the Control of a Multi-Jointed Monoped Runner,” *Proceedings of the IEEE International Conference on Robotics and Automation*, pp. 2676-2682, 1998.
- [19] I. Poulakakis, J. A. Smith and M. Buehler, “Experimentally Validated Bounding Models for the Sout II Quadrupedal Robot,” *Proceedings of the IEEE International Conference on Robotics and Automation*, 2004.
- [20] S. Kajita, T. Nagasaki, K. Yokoi, K. Kaneko, K. Tanie, “Running pattern generation for a humanoid robot,” *Proceedings of IEEE International Conference on Robotics and Automation*, vol. 3, pp. 2755 – 2761, 2002.

- [21] Kale Harbick and Gaurav S. Sukhatme, "Controlling Hopping Height of a Pneumatic Monopod," Proceedings of the IEEE International Conference on Robotics and Automation, pp. 3998-4003, 2002.
- [22] H. Geyer, A. Seyfarth and R. Blickhan, "Natural Dynamics of Spring-Like Running: Emergence of Selfstability," CLAWAR, 2002.
- [23] Robert P. Ringros, "Self-stabilizing running," Ph.D. thesis, Massachusetts Institute of Technology, Cambridge, MA, February 1997.
- [24] T. M. Kubow and R. J. Full, "The Role of the Mechanical System in Control: A Hypothesis of Self-stabilization in Hexapedal Runners," Philosophical Transaction of the Royal Society of London Series B – Biological Sciences, vol. 354, no. 1385, pp. 854-862, 1999.
- [25] T. McGeer, "Passive Bipedal Running", Technical Report, CSS-IS TR 89-02, Centre For Systems Science, Simon Fraser University, Burnaby, BC, Canada, 1989.
- [26] Mojtaba Ahmadi, "Stable Control of a One-Legged Robot Exploiting Passive Dynamics," Ph.D. thesis, Department of Mechanical Engineering, McGill University, Montreal, QC, Canada, March 1998.
- [27] S. Talebi, I. Poulakakis, E. Papadopoulos, and M. Buehler, "Quadruped Robot Running with a Bounding Gait," International Symposium on Experimental Robotics, Honolulu, HI, December 2000.
- [28] Uluc Saranli, Martin Buehler, and Daniel E. Koditschek, "RHex: A Simple and Highly Mobile Hexapod Robot," International Journal of Robotics Research, vol. 20, no. 7, pp. 616-631, July 2001.
- [29] M. Buehler, U. Saranli, and D. E. Koditschek (McGill University, The Regents of the University of Michigan), Single Actuator Per Leg Robotic Hexapod, US Patent, p. 6,481,513 B2, USA, 2002.
- [30] Charles Steeves, "Design and Behavioural Control of a Dynamic Quadruped with Active Wheels," M.Eng. thesis, Department of Mechanical Engineering, McGill University, Montreal, QC, Canada, April 2003.
- [31] Thomas A. McMahon and George C. Cheng, "The mechanics of running: How does stiffness couple with speed?" Journal of Biomechanics, vol. 23, pp. 65-78, 1990.

- [32] Raibert, M. H., Brown, H. B., Jr., Chepponis, M., Hodgins, J., Koechling, J., Dustman, D., Brennan, W. K., Barrett, D. S., Thompson, C. M., Hebert, J. D., Lee, W., and Borvansky, L., "Dynamically Stable Legged Locomotion (September 1985-September 1989)," AI Technical Report 1179, Massachusetts Institute of Technology, MA, USA, 1989.
- [33] E.T. Wittaker and G.N. Watson, "A Course of Modern Analysis," Cambridge University Press, 1902, reprinted 1973.
- [34] Shuuji Kajita, "Dynamic control of a biped in linear inverted pendulum mode," Mechanical Engineering Laboratory Report No. 171, Mechanical Engineering Laboratory, Tsukuba, Japan, March 1996, In Japanese.
- [35] Joel D. Weingarten, Gabriel A. D. Lopes, Martin Buehler, Richard E. Groff, Daniel E. Koditschek, "Automated Gait Adaptation for Legged Robots," Proceedings of the 2004 IEEE International Conference on Robotics and Automation, New Orleans, LA, April 2004
- [36] I. Poulakakis, J.A. Smith, M. Buehler, "On the Dynamics of Bounding and Extensions Towards the Half-Bound and the Gallop Gaits", Proc. of the International Symposium on Adaptive Motion of Animals and Machines (AMAM), Kyoto, Japan, March 2003.
- [37] D. Campbell and M. Buehler, "Preliminary Bounding Experiments in a Dynamic Hexapod," In Bruno Siciliano and Paolo Dario, editors, Experimental Robotics VIII, p. 612-621, Springer-Verlag, 2003.
- [38] Raibert, M. H., Brown, H. B., Jr., Chepponis, M., Hastings, E., Murthy, S. S., Wimberly, F. C., "Dynamically Stable Legged Locomotion--Second Annual Report," CMU--RI--TR--83--1, Robotics Institute, Carnegie-Mellon University, 1983.
- [39] P. Gregorio, M. Ahmadi, and M. Buehler, "Experiments with an Electrically Actuated Planar Hopping Robot," In T. Yoshikawa and F. Miyazaki, editors, Experimental Robotics III, In "Lecture Notes in Control and Information Sciences 200," p. 269-281, Springer Verlag, 1994.

- [40] M. Ahmadi and M. Buehler, "Stable Control of a Simulated One-Legged Running Robot with Hip and Leg Compliance," *IEEE Transactions on Robotics and Automation*, vol. 13, no. 1, pp. 96-104, Feb 1997.
- [41] Brown, H.B., Zeglin, G.Z., "The Bow Leg Hopping Robot," *Proceedings of the IEEE International Conference on Robotics and Automation*, 1998.
- [42] Kale Harbick and Gaurav S. Sukhatme, "Speed Control of a Pneumatic Monopod using a Neural Network," *Technical Report IRIS-02-413*, Institute for Robotics and Intelligent Systems, University of Southern California, 2002
- [43] Koechling and M, H. Raibert, "How fast can a legged robot run?" In *Symposium in Robotics*, DSC-Vol.11, K. Youcef-Toumi, H. Kazerooni (eds.), American Society of Mechanical Engineers, New York, . 1988.
- [44] Matthew D. Berkemeier and Kamal V. Desai, "Control of hopping height in legged robots using a neural-mechanical approach," *Proceedings of the IEEE International Conference on Robotics and Automation*, pp. 1695-1701, 1998.
- [45] Richard Altendorfer, Daniel E. Koditschek, Philip Holmes, "Towards a Factored Analysis of Legged Locomotion Models," *Proceedings of the IEEE International Conference on Robotics and Automation*, pp. 37-44, 2003.
- [46] Eduardo D. Sontag, "A remark on the converging-input converging-state property," *IEEE Transactions on Automatic Control*, vol. 48, no. 2, pp. 313-314, 2003.
- [47] J. P. Ostrowski and J. W. Burdick, "The Control of Mechanical Systems with Symmetries and Nonholonomic Constraints," *Conference on Decision and Control*, 1995.
- [48] Jim Ostrowski and Joel Burdick, "Controllability Tests for Mechanical Systems with Constraints and Symmetries," *Journal of Applied Mathematics and Computer Science*, vol. 17, no. 7, pp. 683-701, July 1998.
- [49] Marc H. Raibert, "Running with symmetry," *International Journal of Robotics Research*, vol. 5, pp. 3-19, 1986.
- [50] Andy Ruina, "The symmetry of some of the simple non-holonomic examples precludes asymptotic stability," *Talk slides*
http://www.tam.cornell.edu/%7Eruina/hplab/nonholonomics_papers.html

- [51] Van der Schaft and H. Schumacher, "An Introduction to Hybrid Dynamical Systems," Lecture Notes in Control and Information Sciences 251, Springer-Verlag, 2000.
- [52] Andrey V. Savkin, Robin J. Evans, "Hybrid Dynamical Systems: Controller and Sensor Switching Problems," Birkhauser, Boston, 2002
- [53] Hui Ye, Anthony N. Michel, Ling Hou, "Stability Theory for Hybrid Dynamical Systems," IEEE Transactions on Automatic Control, vol. 43, no. 4, pp.461-474, April 1998.
- [54] Milos Zefran and Joel W. Burdick, "Design of switching controllers for systems with changing dynamics," Proc. 37th Conference on Decision and Control, pp. 2113-2118, 1998.
- [55] Milos Zefran, Joel W. Burdick, "Stabilization of Systems with Changing Dynamics by Means of Switching," Proceedings of the IEEE International Conference on Robotics and Automation, pp. 1090-1095, 1998.
- [56] Eric Klavins, Haldun Komsuoglu, Robert J. Full and Daniel E. Koditschek, "The Role of Reflexes Versus Central Pattern Generators in Dynamical Legged Locomotion", in J. Ayers and J. Davis editors, Neurotechnology for Biomimetic Robots, MIT Press, 2001.
- [57] MathWorks, Matlab ver. 6.5 and Simulink ver. 4.0, Natick, MA, 2003, <http://www.mathworks.com/>.
- [58] T. W. B. Kibble and F. H. Berkshire, "Classical Mechanics," 4th ed., Addison Wesley, 1997.
- [59] Rodolfo Suarez, Jose Alvarez, Jesus Alvarez, "Regions of Attraction of Closed-Loop Linear Systems with Saturated Linear Feedback," Journal of Mathematical Systems, Estimation, and Control, vol. 5, no. 4, pp. 1-22, Birkhauser-Boston, 1995.
- [60] J-Y. Favez, B. Srinivasan, Ph. Mullhaupt, D. Bonvin, "Condition for Bifurcation of the Region of Attraction in Linear Planar Systems with Saturated Linear Feedback," Proceedings of the 41st IEEE Conference on Decision and Control, Las Vegas, Nevada USA, December 2002.

- [61] H. Michalska, M. Ahmadi, and M. Buehler, "Vertical Motion Control of a Hopping Robot," Proceedings of the IEEE International Conference on Robotics and Automation, pp. 2712-2717, Minneapolis, MN, April 1996.
- [62] William J. Schwind and Daniel E. Koditschek, "Control of Forward Velocity for a Simplified Planar Hopping Robot," Proceedings of the IEEE International Conference on Robotics and Automation, Vol. 1, pp. 691-696, 1995.
- [63] J. Guckenheimer and P. Holmes, "Nonlinear Oscillations, Dynamical Systems and Bifurcations of Vector Fields," Springer-Verlag, 1983.
- [64] J. Koechling, "Gait as Mechanical Oscillation", chapter in Dynamically Stable Legged Locomotion, Robotics Institute Technical Report CMU-LL-4-1985, Carnegie Mellon University, Pittsburgh, 1985.
- [65] Dave McMordie, "Towards pronking with a hexapod robot," Department of Electrical Engineering, McGill University, Montreal, Canada, July, 2002.
- [66] Z. Li and J. He, "An Energy Perturbation Approach to Limit Cycle Analysis in Legged Locomotion Systems", Proceedings of the IEEE International Conference on Robotics and Automation, pp. 1989 - 1994, 1990.
- [67] I. A. Hiskens, "Stability of hybrid system limit cycles: Application to the compass gait biped robot", Proceedings of the 40th IEEE Conference on Decision and Control, Orlando, FL, December 2001.
- [68] T.S Parker and L.O. Chua, "Practical Numerical Algorithms for Chaotic Systems," Springer-Verlag, New York, NY, 1989.
- [69] R. Seydel, "Practical Bifurcation and Stability Analysis," Springer-Verlag, New York, 2nd edition, 1994.
- [70] H. K. Khalil, "Nonlinear Systems," 2nd ed., Prentice Hall, 1996.
- [71] Kuznetsov Y., "Elements of Applied Bifurcation Theory," 2nd ed., Springer-Verlag, 1998.
- [72] Nicholas B. Tufillaro, Jeremiah Reilly, and Tyler Abbott, "An experimental approach to nonlinear dynamics and chaos," Addison-Wesley, 1992.

- [73] Daniel E. Koditschek and Martin Buehler, "Analysis of a Simplified Hopping Robot", *The International Journal of Robotics Research*, vol. 10, no. 6, pp.587 – 605, 1991.
- [74] S.H. Hyon, T. Mita, "Development of a biologically inspired hopping robot - Kenken," *Proceedings of the IEEE International Conference on Robotics and Automation*, vol. 4 , pp. 3984 – 3991, May 2002.
- [75] Gene F. Franklin, J. David Powell, Abbas Emami-Naeini, "Feedback Control of Dynamic Systems," 4th ed., Prentice Hall, 2002.
- [76] Thompson, C. M., Raibert, M. H., "Passive dynamic running," In *International Symposium of Experimental Robotics*, Hayward, V., Khatib, O. (eds.), Springer-Verlag, New York, 1989.
- [77] P. Gregorio, M. Ahmadi, and M. Buehler, "Design, Control, and Energetics of an Electrically Actuated Legged Robot," *IEEE Transactions on Systems, Man, and Cybernetics*, vol. 27B, no. 4, pp. 626-634, Aug 1997.
- [78] Hamidreza Dokht Taghirad, "Analysis, Design, and Control of a Hopping Robot," M.Eng. Project Report, Department of Mechanical Engineering, McGill University, Montreal, QC, Canada, April 1993.